Polymer Testing 159 (2026) 109181

Contents lists available at ScienceDirect

Polymer Testing

journal homepage: www.elsevier.com/locate/polytest

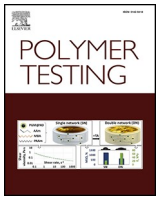

Comprehensive investigation of thermal aging mechanisms in PFA for high-voltage cable insulation in hybrid-electric aircraft

Jawad Ahmad *, Mohamad Ghaffarian Niasar

High Voltage Technologies, Department of Electrical Sustainable Energy, Delft University of Technology, Delft, 2628 CD, the Netherlands

ARTICLE INFO

Keywords:
PFA aircraft cables
Thermal oxygen aging
Chemicrystallization
Chain scission
Dynamic mechanical analysis
Dielectric strength
Thermal stability
MDS

ABSTRACT

Perfluoroalkoxy alkane (PFA) is a promising candidate for onbaord high-voltage cable insulation due to its superior dielectric properties, chemical resistance, and high thermal stability. Understanding the thermal aging behavior of PFA is essential for ensuring the long-term reliability of insulation materials in hybrid-electric aircraft, where high thermal fluctuations are common. This study investigates the chemical, structural, mechanical, and dielectric properties of PFA aged at 280 °C for up to 1000 h, simulating real-world aerospace operational environments. Results show that PFA undergoes chain scission and chemicrystallization in the early aging stages (0-480 h), leading to an increase in crystallinity. However, at longer aging times e.g. (>480 h), oxidative degradation becomes dominant, resulting in chemical and structural changes correlated with microstructural damage, including crack formation, tie-chain loss, and lamellar disruption. Dynamic mechanical analysis and tensile results show a significant decrease in molecular rigidity with a reduction in glass transition temperature (T_g), indicating a loss of material stiffness and a reduction in tensile strength (42.16%) and elongation (30.2%) after long term exposure (1000 h). Dielectric characterization demonstrates monotonic increase in dielectric constant (from 1.90 to 2.15), dissipation factor, and AC conductivity, attributed to the formation of polar oxidation products and defect-assisted interfacial polarization. The dielectric strength also decreases from 95.2 kV/mm to 87.1 kV/mm after 1000 h of aging. Molecular dynamics simulations (MDS) are also performed to study the temperature effect on PFA, revealing that at high temperatures, the PFA molecular structure is increasingly destroyed by thermal chain scission. These findings provide valuable insight into the degradation mechanisms governing PFA performance and contribute to evaluating its reliability as an insulation material for high-voltage cable systems in hybrid-electric aircraft.

1. Introduction

The rapid shift toward aircraft electrification driven by the need to reduce fuel consumption, emissions, and operating costs is fundamentally transforming the electrical power architecture of modern aviation. Hybrid-electric propulsion concepts and fully electric aircraft require unprecedented levels of onboard electrical power, with distribution systems expected to operate at voltage levels approaching 1 kV and power ratings reaching several megawatts [1]. These elevated electrical and thermal loads impose stringent demands on cable insulation systems, making the long-term reliability of polymeric insulation a critical factor in the safe operation of future electric aircraft.

Current aerospace wiring relies heavily on high-performance fluoropolymers and engineering plastics due to their excellent dielectric strength, thermal endurance, and chemical resistance. Commonly used materials include polytetrafluoroethylene (PTFE), fluorinated ethylene propylene (FEP), ethylene tetrafluoroethylene (ETFE), polyimide (PI), Polyether ether ketone (PEEK) and perfluoroalkoxy alkane (PFA) [2,3]. In addition to fluoropolymers, silicone-based polymers have also been widely investigated as electrical insulation materials because of their flexibility and dielectric stability. Recent studies have focused on improving the dielectric strength and thermal conductivity of silicone systems through composite engineering using inorganic fillers or electron-acceptor additives [4,5]. While these approaches can enhance dielectric performance, silicone materials generally exhibit lower intrinsic thermal stability and may suffer structural degradation under prolonged high-temperature exposure. In contrast, fluoropolymers such as PFA (having a continuous service temperature up to 260 °C) possess exceptional thermal endurance, excellent chemical resistance, and inherently low dissipation factor due to their highly fluorinated

* Corresponding author.
E-mail address: J.ahmad@tudelft.nl (J. Ahmad).

https://doi.org/10.1016/j.polymertesting.2026.109181
Received 9 January 2026; Received in revised form 12 April 2026; Accepted 14 April 2026
Available online 19 April 2026

molecular structure. These intrinsic properties allow PFA to maintain stable electrical insulation performance at elevated temperatures without the need for complex filler modifications. Also, PFA combines the inertness and electrical stability of PTFE with improved melt-processability and mechanical robustness making it particularly attractive for high-voltage aerospace wiring systems [6,7].

During aircraft service operation, electrical systems are subjected to a broad range of environmental conditions, including temperature variations from approximately −85 °C to 300 °C, pressure fluctuations between 1 and 0.2 atm, varying humidity levels, and significant mechanical vibrations associated with flight operation [8]. Aviation cable standards indicate that electrical wiring should tolerate temperatures from approximately −65 °C to at least 150 °C under normal service conditions [1]. In hybrid-electric propulsion architectures, however, short-duration overload events may occur during high-power operating phases such as takeoff or initial climb, which can temporarily increase the thermal stress on aircraft cabling systems. These thermal stresses may further accelerate aging and degradation processes in the insulation system. Previous studies have shown that prolonged exposure to elevated temperatures can induce chain scission, oxidation, microvoid formation, and changes in crystallinity, which collectively deteriorate the mechanical, thermal, and dielectric performance of insulation materials [8,9]. As electrified propulsion concepts push cable operating conditions closer to the upper thermal limits of insulation materials, understanding the long-term aging behavior of PFA becomes increasingly important.

Previous studies on aerospace insulation have primarily focused on materials such as PTFE, PEEK, and PI, revealing significant degradation of mechanical strength, dielectric performance, and microstructural integrity under thermal oxidative exposure. However, systematic studies on the thermal aging behavior of PFA particularly in the context of aircraft high-voltage cable insulation remain very limited. Indeed, very few investigations have been carried out into the thermal aging performance of PFA covering the comprehensive study of physical, chemical and dielectric properties of PFA. It has been reported that that the high-temperature exposure above 200 °C leads to gradual chain scission and accelerates degradation in PFA, producing new reactive functional groups that can compromise the conductivity of PFA [9]. Another study presented the effect of thermal aging on dielectric breakdown and thermal stability performance of PFA [10]. The thermal pyrolysis in PFA resulted in generation of free radicals due to chain scission phenomenon. No, further studies on the degradation behavior of PFA under prolonged thermal stress are available in literature. As PFA becomes increasingly adopted in high-voltage aerospace wiring, there is a pressing need to evaluate how its physicochemical properties evolve under long-term thermal oxidative stress.

In this work, a comprehensive investigation of the thermal aging behavior of PFA films is conducted to assess their suitability for next-generation aircraft high-voltage cable insulation. The study examines changes in chemical structure, surface morphology, crystallinity, thermal stability, molecular mobility, mechanical performance, dielectric properties, and AC dielectric strength following controlled thermal exposure at 280 °C above service temperature of PFA. By correlating these multi-scale degradation phenomena, this research provides critical insights into the long-term reliability of PFA under elevated thermal stress and offers valuable guidance for the design, qualification, and application of PFA insulated high-voltage cables in future electrified aircraft.

2. Experimental and methodologies

2.1. Materials

Perfluoroalkoxy alkane (PFA) films were sourced from Holscot Europe B.V. (Breda, Netherlands). The films were supplied with dimensions of 200 mm × 140 mm and a thickness of 0.1 mm. The films were manufactured from high-purity PFA resin, which is known for its excellent physicochemical stability, chemical inertness, and exceptional thermal endurance, with a continuous service temperature range from −254 °C to +260 °C.

2.2. Acceleration thermal aging

PFA films were first cleaned with isopropyl alcohol, and dried using lint-free cloth. The specimens were mounted on wire-mesh racks, maintaining a minimum clearance of 5 cm from the oven walls to prevent contact and to ensure uniform airflow, as illustrated in Fig. 1. The racks were then placed in a convection oven set to 280 °C. A temperature above the nominal service limit of PFA (260 °C) was selected to accelerate the thermal-oxidative aging process. The cyclic thermal profile, consisting of repeated thermal cycles (shown in Fig. 1) was selected to better represent realistic temperature conditions in aerospace environments where insulation materials undergo repeated heating and cooling cycles rather than continuous high-temperature exposure. Each cycle includes 8 h of exposure at 280 °C followed by 16 h of natural cooling to room temperature, resulting in a 24-h cycle. This sequence was repeated for a total of 42 cycles (~1000 h total aging duration).

Aging intervals were selected corresponding to the aging times (240 h, 480 h, 720 h, and 1000 h) which represents the total duration of the cyclic aging profile e.g. the cumulative thermal exposure at 280 °C is 336 h for the longest aging condition (1000 h). The samples were finally removed from the oven (at these designated aging intervals 240 h, 480 h, 720 h, and 1000 h), cooled under ambient conditions, and subsequently subjected to mechanical, thermal, dielectric, and chemical characterization.

2.3. Fourier transformed infrared (FTIR) spectroscopy

FTIR spectra of PFA samples were recorded in the range of 4000–400 cm^{-1} using a PerkinElmer Spectrum 100 spectrometer operated in transmission mode. A spectral resolution of 4 cm^{-1} was employed, and each spectrum represents an average of 20 scans. Atmospheric background spectra were measured prior to each acquisition and automatically subtracted from the sample spectra to ensure accurate baseline correction.

2.4. surface morphology

Surface morphology was examined using a JSM-7500F field-emission scanning electron microscope. Samples were sputter-coated with a thin layer of gold to minimize surface charging and imaged at an accelerating voltage of 5 kV. For each aging condition, five SEM micrographs were recorded and analyzed to quantify crack features including crack length, width, and spatial distribution using image analysis software (ImageJ) as illustrated in Supplementary Figure S1. Elemental and microstructural information was obtained using energy-dispersive spectrometer (EDS) from Bruker, enabling analysis of the surface chemical composition of the PFA films across different aging conditions.

2.5. thermal properties

Differential scanning calorimetry (DSC) and thermogravimetric analysis (TGA) were employed to evaluate the heat-flow behavior and thermal stability of PFA. DSC was performed using a TA Instruments mDSC 250 system, while TGA was conducted on a PerkinElmer TGA 4000 instrument. Samples weighing 8-10 mg were heated under a nitrogen atmosphere at a rate of 10 °C/min. For DSC measurements, the temperature was increased from room temperature to 350 °C, followed by cooling at 10 °C/min back to ambient conditions. For TGA measurements, samples were heated from room temperature to 700 °C at the same heating rate to obtain thermal degradation profiles.

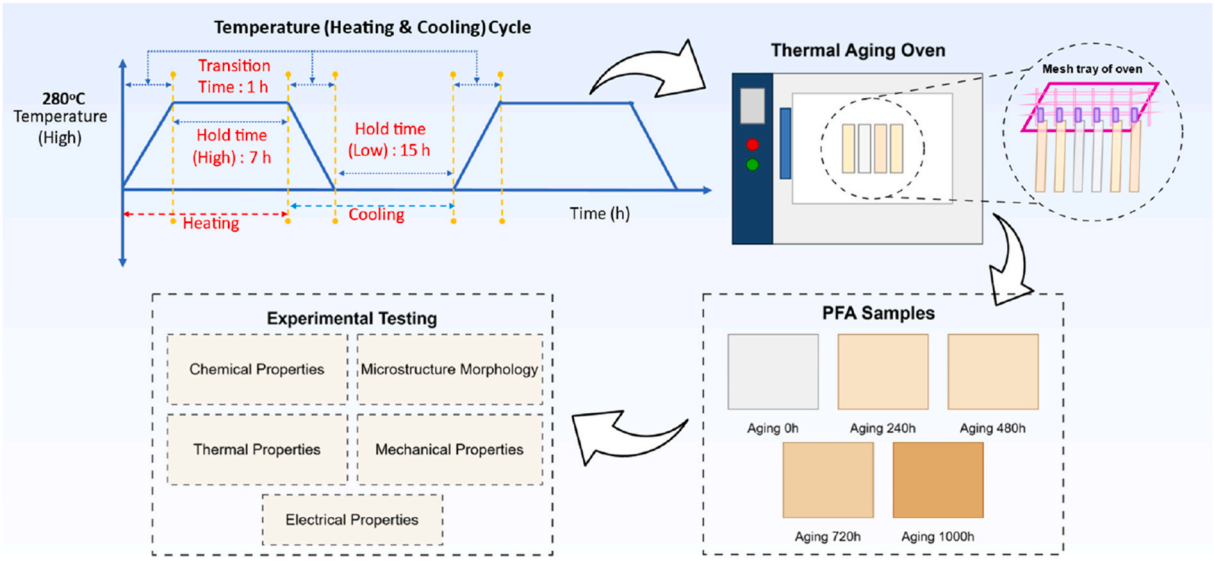

Fig. 1. PFA accelerated thermal aging flowchart.

2.6. mechanical properties

Tensile specimens were cut into a standardized dumbbell geometry using a laser cutter, as shown in Supplementary Figure S2. Mechanical testing was performed at room temperature on a Zwick Universal Testing Machine equipped with a 1 kN load cell and a crosshead speed of 10 mm/min. An extensometer was attached directly to the gauge section of each specimen to accurately record strain and displacement during loading. Stress–strain curves were obtained and used to determine tensile strength (MPa) and elongation at break (%). For each aging condition, five consecutive measurements were performed, and the mean values with associated errors were reported. Dynamic mechanical analysis (DMA) was conducted using a TA Instruments RSA-G2 system in tension mode at 1 Hz. The samples were heated from room temperature to 250 °C under a controlled temperature ramp, enabling evaluation of viscoelastic responses and molecular mobility in the aged and unaged PFA specimens.

2.7. dielectric properties

Dielectric properties including dielectric constant, dissipation factor, AC conductivity, and volume resistivity were measured using a Novocontrol Concept 80 broadband dielectric analyzer at room temperature over a frequency range of 10^{-1} to 10^{6} Hz using an applied voltage of 1 Vrms. For AC dielectric strength testing, PFA films were cut into circular specimens of suitable diameter and evaluated using the high-voltage dielectric breakdown setup shown in Supplementary Figure S3. Synthetic ester insulating oil (Midel 7131) was used as the surrounding medium to suppress surface discharges and prevent flashover. Dielectric strength was measured at room temperature, and five repeated tests were conducted for each aging condition to obtain the average value.

2.8. molecular dynamics simulation based on reactive force field (ReaxFF-MD)

A reactive molecular dynamics (ReaxFF-MD) simulation was conducted to examine the temperature-dependent structural evolution of PFA polymer, given the strong relationship between polymer microstructure and electrical properties. Temperature models were prepared at 25 °C, 120 °C, 260 °C, 280 °C, and 300 °C, covering both the experimental aging condition (280 °C) and a temperature near the melting point of PFA (300 °C). A PFA polymer chain and lattice cell ($40.5 \times 40.5 \times 40.5$ Å^3) as shown in Supplementary Fig. S4 was first constructed in Materials Studio, where all temperature-specific structures were geometry-optimized using the CVFF (Consistent Valence Force Field) to remove steric and mechanical instabilities. Free volume of PFA was calculated at all mentioned temperatures in Material Studio. The optimized models were additionally imported into large scale Atomic/Molecular massively parallel simulator (LAMMPS), where ReaxFF was applied to capture temperature-induced bond-order changes and potential degradation pathways. Each system was equilibrated under an NVT (constant Number of particles, Volume, and Temperature) ensemble for 1000 ps to obtain stable configurations and evaluate binding and activation energies. All simulations were performed using 24 CPU (Central Processing Unit) cores to ensure computational efficiency.

3. Results and discussion

3.1. FTIR analysis

To better visualize the relative evolution of characteristic functional groups during aging, the FTIR spectra were normalized using the C–O–C ether stretching band (995 cm^{-1}), and the normalized spectra are presented in Fig. 2(a).

Unaged PFA shows a sharp band at around 995 cm^{-1} as shown in Fig. 2(a) which is attributed to the C–O–C stretching in ether groups [11] and two strong bands at 1145–1200 cm^{-1} are related to C–F stretching vibration in CF_2 backbone and CF_3 side groups [12,13]. The characteristic peaks captured at 720, 740, and 778 cm^{-1} are due to wagging and rocking modes of CF_2 groups present in the amorphous regions of PFA, while contributions from CF_3 bending vibrations are also present in this region [14,15]. The change in the intensity of these bands is correlated with the changes in crystallinity of the PFA. It can be seen that bands intensity of these bands decrease with aging time. These changes are indicative of a possible decrease in the amorphous part, which can be related to increase in crystallinity of PFA during aging process [8]. Peaks from 600 to 650 cm^{-1} are due to CF_2 bending. It can be noticed from Fig. 2(a) that the peak intensities observed at 1200 cm^{-1} and 1146 cm^{-1} are decreased with increasing aging time which is indicative of the reduction in the number of CF_2 and CF_3 groups during aging. The relative decrease in the CF_2 backbone stretching band and the CF_3 side-group band becomes more apparent with increasing aging time. Indeed, the CF_2 backbone and CF_3 side-group peaks decrease more noticeably than the CF_2 bending and wagging/rocking modes, which exhibit comparatively smaller variations. These observations suggest

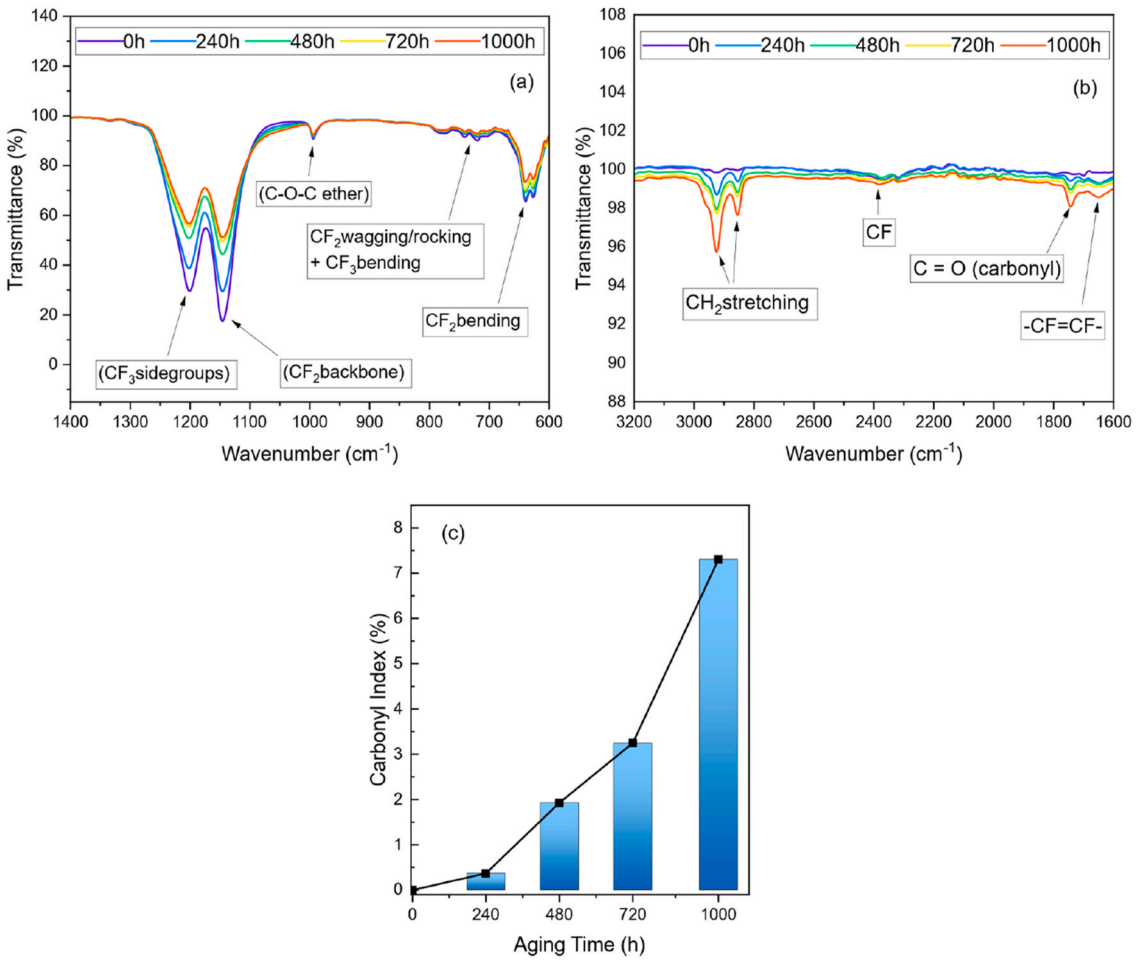

Fig. 2. PFA FTIR spectra (a) 1400-600 cm^{-1} (b) 3200-1600 cm^{-1} (c) CI with aging time.

that thermo-oxidative aging preferentially affects the backbone and ether side-chain fluorinated units of PFA. Weakening of C–F and C–O–C provides a clear signature of degradation of PFA.

New peak at 1743 cm^{-1} as shown in Fig. 2(b) represents the C=O stretching (carbonyl) which is related to the COOH groups. The peaks are more pronounced at the later stage of aging e.g. 720-1000 h due to the degradation of the PFA molecular chains during the thermal aging process [16]. A small peak at 2353 cm^{-1} belongs to the -C-F bond absorption [17]. In the higher wavenumber region (2800–3000 cm^{-1}), new absorption bands corresponding to CH_2 stretching vibrations are observed. The band near 2924 cm^{-1} is attributed to asymmetric CH_2 stretching, while the band around 2854 cm^{-1} corresponds to symmetric CH_2 stretching. These changes are indicative of surface oxidation or adsorbed species in PFA. In addition to these peaks, another weak peak was observed at 1645 cm^{-1} which is attributed to the stretching vibration of the –CF = CF–group [18]. The appearance of these absorption bands is attributed to degradation of the fluoropolymer structure, arising from homolytic bond cleavage within the polymer backbone [19]. The presence of these groups is attributed mainly to products of chain scissions and oxidation reactions by oxygen present in air during thermal oxidative aging, which leads to the formation of double bonds by bond retraction [20,21]. To study the PFA polymer oxidation or degradation, the carbonyl index is used and calculated using the following [22,23]:

$$\text{Carbonyl Index (CI) (\%)} = \frac{A1743}{A1145} \text{ x } 100\% \quad (1)$$

A1743 is the peak area of the carbonyl stretching vibration peak at 1743 cm^{-1} and A1145 represents the peak area of CF_2 peak standard at 1145 cm^{-1}. The change of carbonyl index change of PFA after thermal aging is highlighted in Fig. 2(c). It can be noticed from Fig. 2(c) that with the increase of thermal aging time from 0 h to 480 h, CI steadily increases step wise from 0% to 1.93%. This indicates that under the action of thermal aging, the weak bonds of PFA macromolecular chains are broken and substances containing carbonyl groups are generated. The carbonyl index increases sharply after 480 h of aging, reaching 7.30% at 1000 h demonstrating that oxygen was involved in the degradation process. This means that at the later stage of aging process e.g. 720-1000 h, PFA is more seriously affected by the thermal oxygen effect resulting in a higher carbonyl index. Perhaps, the ether group can be attacked during the aging process and COOH groups can be introduced [16,24].

3.2. *Microscopic surface morphology*

The formation of micro-voids within the polymer film significantly influences its electrical characteristics. The presence of such micro-cavities in the polymer plays a critical role in interpreting variations in high-voltage performance and overall insulation behavior [25]. To investigate the effect of thermal aging on the microscopic morphology of PFA, SEM micrographs were obtained at identical magnifications as shown in Fig. 3.

The SEM micrographs of PFA reveal a gradual but distinct evolution in surface morphology with increasing exposure time. The surface of the pristine PFA (0 h) exhibited a smooth and uniform texture whereas the aged samples progressively developed a rough and irregular appearance as highlighted in Fig. 3. At 240 h, the surface of PFA appears

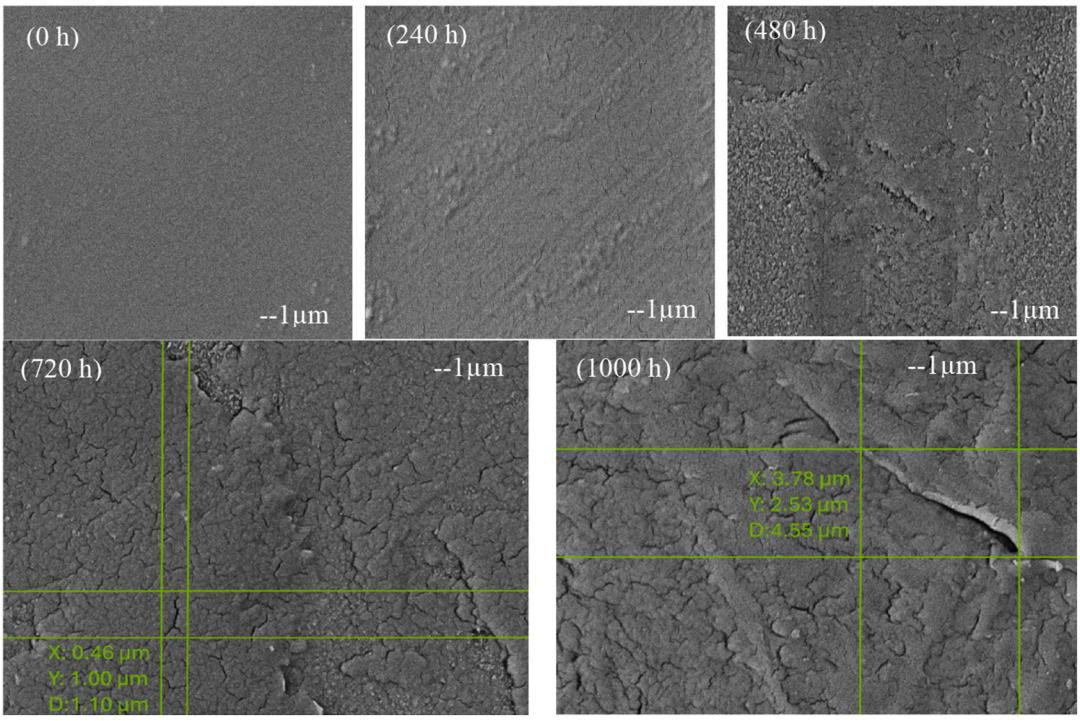

Fig. 3. PFA SEM surface microstructure morphology vs aging time.

comparatively rough with no visible cracks or pit holes. After 480 h of aging process, the surface remains largely continuous, showing only mild roughness and a few shallow groove-like features, indicating the onset of thermal relaxation and early chain scission. At 720 h, the PFA polymer surface becomes noticeably rougher, with fine micro-cracks and surface undulations suggesting the progression of thermally induced degradation and partial molecular rearrangement. By 1000 h, the deterioration becomes pronounced with dense, sharp and interconnected cracks appear, accompanied by surface peeling, pits, and voids as highlighted in Fig. 3. These features reflect advanced chain scission, oxidative attack, and localized mass loss, leading to embrittlement and severe loss of surface integrity. The micro-voids are likely associated with the formation of low-molecular-weight fluorinated fragments during prolonged thermal aging that may diffuse out of the polymer matrix and locally reduce the material density. Overall, the morphological evolution from a smooth, intact surface to a heavily cracked structure highlights the cumulative impact of prolonged high-temperature exposure on the microstructural stability of PFA insulation.

3.2.1. *Surface crack evolution and quantitative analysis*

Quantitative crack analysis has been performed (shown in Fig. 4(a and b) to further support the morphological degradation observed in the SEM images of PFA aged samples (720 h and 1000 h). The crack length and width distribution plots are shown in Fig. 4(c–f) and corresponding data with standard deviations (σ) are given in Table 1. For the PFA sample aged for 720 h, the average crack length and width were calculated as 0.34 μm and 0.045 μm as shown in Fig. 4(c and d), respectively, with a maximum crack length of 1.50 μm. The total crack count was 229, indicating the presence of isolated and fine surface fissures. After 1000 h of thermal exposure, both the number and dimensions of cracks increased noticeably. The maximum crack length of PFA samples after 1000 h reached 4.77 μm, while the average width expanded to 0.053 μm (Fig. 4(f)), with 249 cracks counted. This progressive increase in crack size and density demonstrates that extended aging promotes micro-void coalescence and crack propagation in PFA surface as a result of cumulative chain scission and oxidative degradation. The enlargement of crack dimensions reflects a decline in surface cohesion and the transition from micro-defect initiation to macroscopic fracture features, thereby indicating the severe embrittlement and loss of mechanical integrity of the PFA polymer at prolonged exposure durations. These aging induced surface cracks may facilitate moisture ingression into the PFA bulk in presence of humid environmental conditions.

3.2.2. *EDS scan analysis*

EDS surface analysis (see Supplementary Fig. S5) reveals clear thermal-oxidative degradation of PFA during aging at 280 °C at higher exposure time e.g. 1000 h. The atomic fraction of fluorine decreases from 68.29% (0 h) to 66.19% (1000 h) as shown in Table 2, while oxygen simultaneously increases from 3.44% to 5.05%. Using the more reliable elemental ratios, the F/C ratio progressively decreases from 2.42 (0 h) to 2.30 (1000 h), indicating defluorination caused by C-F bond scission and volatilization of fluorinated fragments in PFA. In contrast, the O/C ratio increases by ~50% from 0.12 (0 h) to 0.18 (1000 h), demonstrating oxidative enrichment of the surface and formation of oxygenated functionalities such as carbonyls. These chemical signatures confirm that PFA undergoes oxidative chain scission, which is known to preferentially attack the amorphous phase and tie-macromolecules. The chemical changes observed in PFA by EDS correspond directly with the morphological alterations detected under SEM. These morphological features are consistent with chain scission, shrinkage stresses, and lamellar disintegration, confirming significant loss of mechanical connectivity in the semi-crystalline structure of PFA. The loss of fluorinated fragments may expose the PFA polymer bulk to further degradation as presence of fluorine layer usually protects the polymer surface from further degradation into the polymer bulk [8].

To assess possible diffusion-limited oxidation (DLO), The EDS for PFA cross-section was also performed and EDS analyses were compared between the surface and cross-section of the aged PFA film. After 1000 h aging, the surface shows slightly higher oxygen (5.1%) and lower fluorine (66.2%) than the bulk region (O = 4.8% and F = 67.4%), indicating mild surface-preferential oxidation. This is further supported by elemental ratios in Table 3. The bulk O/C ratio increases 46.5% after (1000 h) compared to the surface O/C ratio (50%), confirming oxidative

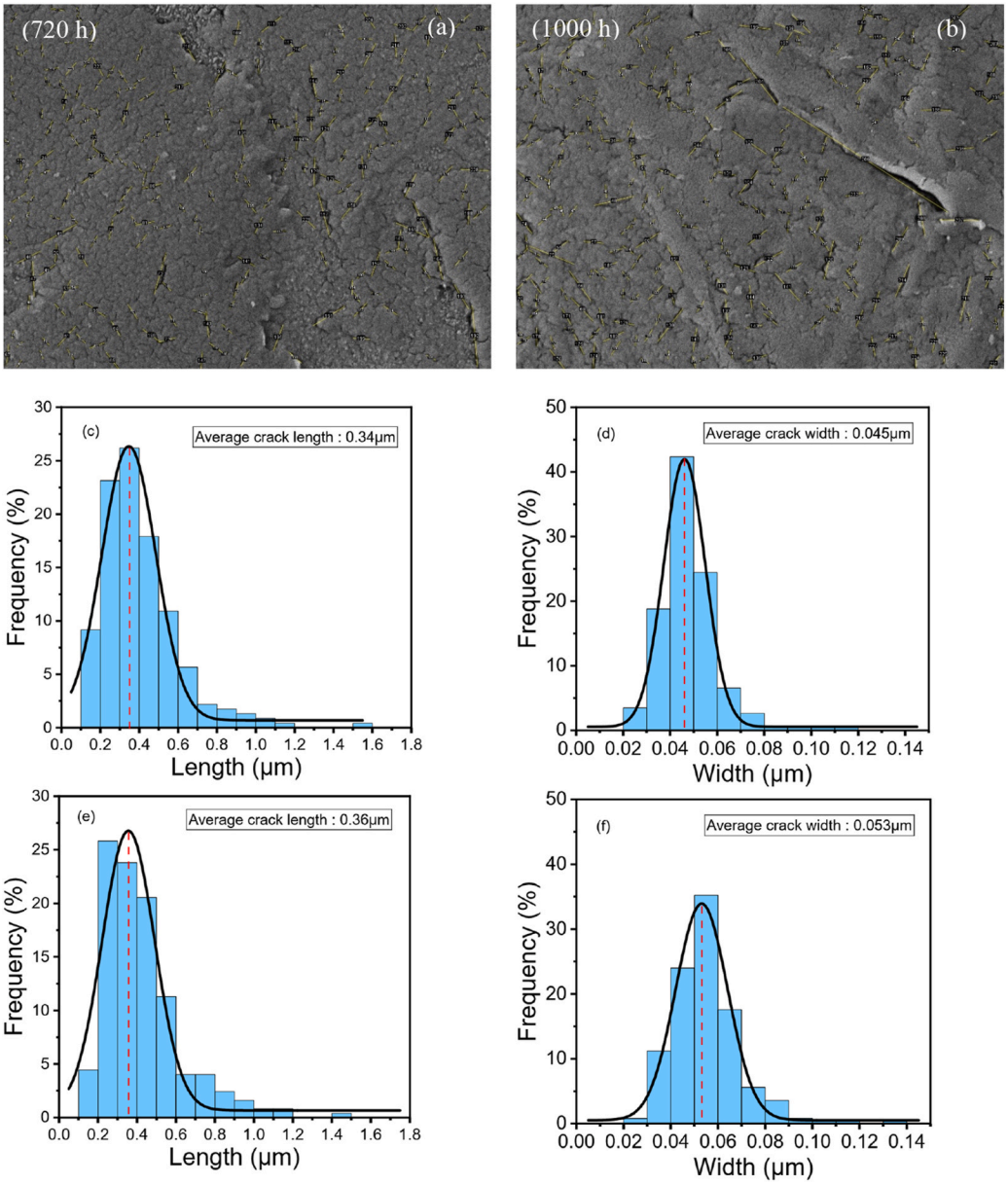

Fig. 4. PFA SEM surface crack size distribution vs aging time (a) 720 h, (b) 1000 h, (c-d) crack length and width distribution of PFA (720 h), (e-f) crack length and width distribution of PFA (1000 h).

Table 1
Surface crack size distribution of PFA samples.

Samples	Crack Length (μm)			Crack Width (μm)			Number of Cracks (counts)
	Max	Average	σ	Max	Average	σ	
PFA (720 h)	1.50	0.34	0.09	0.11	0.045	0.008	229
PFA (1000 h)	4.77	0.36	0.10	0.14	0.053	0.010	249

Table 2
EDS surface scan data of PFA samples.

Elements	Weight (%)		Atomic (%)	
	0 h	1000 h	0 h	1000 h
C	20.1	20.5	28.3	28.7
O	3.2	4.8	3.4	5.1
F	76.7	74.7	68.3	66.2

Table 3
EDS cross-sectional (bulk) scan data of PFA samples.

Elements	Weight (%)		Atomic (%)	
	0 h	1000 h	0 h	1000 h
C	19.7	20.0	27.5	27.8
O	3.0	4.6	3.2	4.8
F	77.3	75.4	69.3	67.4

enrichment in both regions with a slightly stronger effect at the surface. At the same time, the bulk F/C ratio decreases 3.9% after (1000 h), compared with a decrease of 4.5% at the surface, suggesting stronger surface defluorination and/or volatilization of fluorinated fragments near the exposed surface. Cross-sectional SEM images in (see Supplementary Figure S6) provide further insight into the microstructural evolution of PFA during thermal aging. The unaged PFA (0 h) exhibits a dense and uniform cross-section without visible defects. After 1000 h aging at 280 °C, significant morphological changes are observed. Surface regions display pronounced cracking and delamination, indicating oxidation-induced embrittlement and microstructural damage. In contrast, the interior region remains comparatively more continuous, although increased roughness and microvoids are present (visible in high-contract image in Supplementary Fig. S6), suggesting that degradation also occurred within the bulk material. These observations indicate that oxidation is somewhat more pronounced at the exposed surfaces. However, because the differences between surface and bulk remain small and no thick oxidized skin layer is observed, severe diffusion-limited oxidation appears to be limited in the 0.1 mm PFA film.

3.3. Proposed degradation mechanism of PFA during thermal aging

3.3.1. Stage I: 0–480 h — thermally driven chain scission and structural rearrangement

In the early stage, the degradation of PFA is proposed to initiate at vulnerable bonds located near the side-chain region (–O–CF_2–) containing ether linkages, where thermal stress weakens the C–O–C bonds and adjacent backbone bonds (C–C) as schematically shown in Fig. 5. This generates radical species and shorter fluorinated chain fragments. These radicals can undergo β-scission or unzipping reactions, producing unsaturated fluorinated end groups such as -CF=CF_2. This interpretation is consistent with the gradual weakening of the C-O-C ether band in the FTIR spectra, indicating cleavage of the ether-containing structure and partial loss of intact CF_2/CF_3 environments. As said earlier in FTIR analysis that the decrease in the 720–778 cm^{-1} bands, mainly associated with CF_2 wagging/rocking vibrations in the amorphous phase, suggests a reduction of amorphous content and rearrangement of shortened chains, i.e. chemi-crystallization. During this stage, oxidation is still limited, as reflected by the relatively small increase in carbonyl index up to 480 h in FTIR. Therefore, the dominant mechanism in Stage I is thermal chain scission and chain rearrangement, rather than oxidation.

3.3.2. Stage II: 480-1000 h — thermo-oxidative degradation

At longer aging times, oxygen becomes increasingly involved in the degradation process as shown in Fig. 5. The radical and unsaturated fluorinated intermediates formed in Stage I provide reactive sites for oxygen attack, leading to oxidized species such as acyl fluoride groups (Rf-COF). Similar kind of oxidation markers are observed in degradation pathways of fluorinated polymers reported in the literature [19,26].

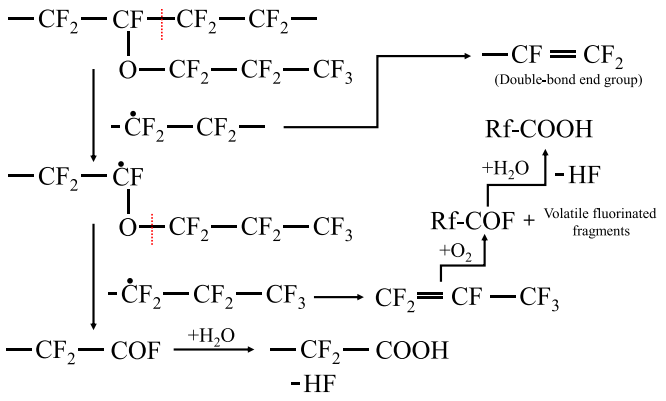

Fig. 5. Possible degradation reactions in PFA due to aging.

These species may further hydrolyze to carboxylic acid groups (Rf-COOH) with release of HF [27,28]. This hydrolysis reaction can occur in the presence of trace moisture, which may originate from ambient humidity absorbed by the samples during the cooling stage or subsequent handling. This transition is strongly supported by the FTIR results in the 1600–3200 cm^{-1} region, where the carbonyl band around 1743 cm^{-1} becomes progressively stronger. The carbonyl index increased sharply after 480 h, confirming that thermo-oxidative degradation becomes dominant in the later stage. The EDS results further supported this interpretation: the fluorine atomic fraction decreases while the oxygen content increases, indicating both defluorination and oxidative enrichment. These results are consistent with the formation of oxygen-containing functionalities and the volatilization of fluorinated fragments generated during oxidative chain scission. Regarding the competition between chain scission and crosslinking, the present results indicate that chain scission is the dominant mechanism. This is supported by the weakening of characteristic FTIR backbone bands, the growth of carbonyl-containing products, the EDS evidence of fluorine loss and oxygen uptake, and the severe cracking and embrittlement seen in SEM. Although transient radical recombination cannot be completely ruled out, there is no direct evidence in the present work that crosslinking is a dominant pathway. Instead, the radicals generated during thermal cleavage are more likely to undergo β-scission, unzipping, and oxygen-assisted oxidation, which ultimately produce oxidized fragments and microstructural damage.

3.4. Thermal properties (TGA & DSC analysis)

To evaluate the thermal stability of PFA samples, some important parameters e.g. thermal decomposition temperature at 5% weight loss ($T_{5\%}$), decomposition temperature at 30% weight loss ($T_{30\%}$) maximum decomposition temperature (T_{max}) are listed in Table 4. In general, materials with high heat resistance and long molecular chain results in high decomposition temperature [8]. TGA curves of PFA appear stable with no weight loss observed until 470 °C as shown in Fig. 6(a). PFA samples show a clear one step decomposition with a rapid and substantial mass loss observed after 500 °C and the entire mass loss occurs during this process until 600 °C leaving no residual mass (R_w). The aged PFA samples show earlier onset of thermal decomposition ranging ($T_{5\%}$) from 502.0 °C to 496.1 °C as compared to pristine PFA which is 504.7 °C, reflecting the formation of low-molecular-weight and volatile oxidation products generated through chain scission. With the increase of aging time from 240 to 1000 h, the DTG peak temperature (T_{max}) also shifts downward (from 553.6 °C to 548.1 °C) as shown in Fig. 6(b), indicating that the main decomposition event requires less thermal energy in aged PFA samples. This is consistent with oxidative degradation, defluorination, and reduced average molecular weight, all of which lower the activation energy for decomposition resulting in faster and earlier decomposition. The heat-resistance index (THRI) is used to analyze the thermal stability of the PFA samples, and the results are in given in Table 4 [29,30]. As shown in Fig. 6(c), the THRI value for unaged PFA is about 256.9 °C, and it decreases in case of aged samples ranging from 255.9 °C (240 h) to 252.6 °C (1000 h). This indicates that the aging has accelerated the thermal decomposition of PFA and thermal stability of PFA is steadily decreased due to the destruction of PFA molecular chain caused by thermo-oxidative aging.

Table 4
TGA & DTG data of PFA samples.

Aging time (h)	$T_{5\%}$ (°C)	$T_{30\%}$ (°C)	T_{max} (°C)	THRI (°C)
0	504.7	537.3	554.5	256.9
240	502.0	535.8	553.6	255.9
480	500.1	533.8	552.2	254.9
720	498.6	531.7	549.5	254.0
1000	496.1	528.6	548.1	252.6

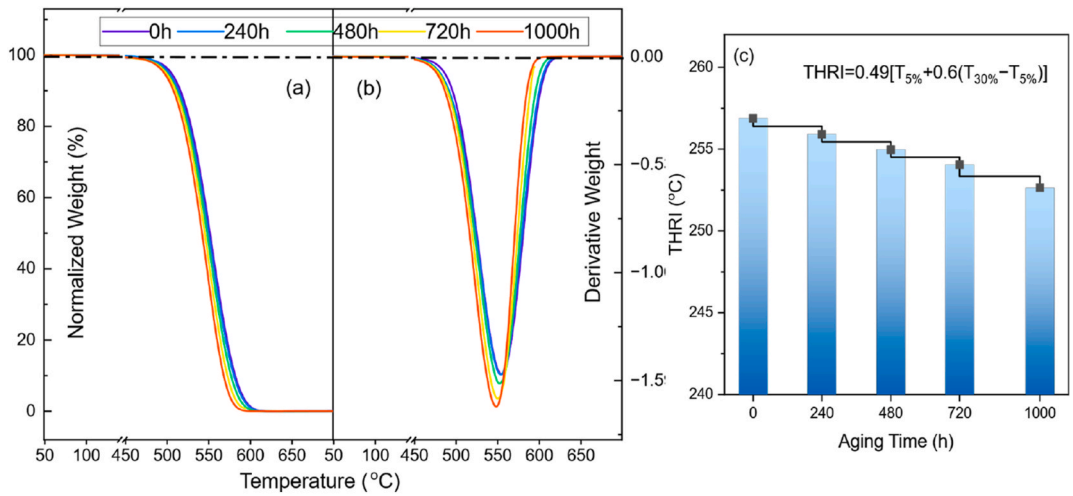

Fig. 6. Thermal decomposition curves of PFA samples (a) TGA, (b) DTG, (c) THRI.

The effect of thermal aging on the melting and crystallization behavior of PFA samples is studied. The evolution of DSC melting and crystallization peaks observed in aging period 0-1000 h is highlighted in Fig. 7. The essential parameters of DSC heating and cooling curves e.g. melting temperature (T_m), enthalpy of fusion or melting peak area (ΔH_m), crystallization temperature (T_c), cooling peak area (ΔH_c) and crystallinity (X_c) obtained from analysis are listed in Table 5. The test crystallinity X_c of PFA samples is determined using Equation (2).

$$X_c\ (\%) = (\Delta H_m / \Delta H_m^0) \times 100 \quad (2)$$

where ΔH_m is the enthalpy of fusion measured by DSC and ΔH_m^0 is the melting enthalpy of 100% crystalline PFA i.e. 67 J/g [11,31].

It can be seen from the results that the DSC melting and crystallization peaks of PFA are getting sharper in early stage of aging process (0-480 h). A clear increase of melting point from 307.7 °C to 310.0 °C is observed in early aging period (0-480 h). The melting enthalpy (ΔH_m) obtained from the heating scan increases from 22.9 J/g to 31.0 J/g during the early aging period (0-480 h), and the corresponding crystallinity increases from 34.2% to 46.2%. Since these values are calculated from the heating endotherm, they represent the microstructure of the specimens before thermal history erasure, whereas the cooling scan parameters describe recrystallization from the melt. The increase in crystallinity can be attributed to thermally induced chain scission occurring primarily in the amorphous regions of PFA, particularly near the ether-containing side-chain structures and adjacent backbone bonds. Such cleavage produces shorter molecular segments that enhance chain mobility and facilitate recrystallization in the amorphous regions upon slow cooling from the melting point [32,33]. Molecular weight decreases resulting in better packing of PFA polymer chains leading to creation of more stable crystals that melt at higher temperature [24,34,35]. At higher stage of aging e.g. 720-1000 h, DSC melting curves show a broader distribution with a decrease in melting point, ΔH_m and crystallinity of PFA is observed which can be attributed to the advanced degradation stage. The crystallinity of PFA drops to 40.9% after 1000 h of aging process. Chain scission phenomenon in PFA becomes critical at higher stage of aging time e.g. 1000 h leading to formation of more reactive functional groups and the release of degradation products as discussed in FTIR which may disrupt the crystalline phase and comprise the crystallinity of PFA. The fragmented and disordered chain fragments, as a result of sever chain scission and oxidation, are difficult to crystallize at a later stage of aging process (720-1000 h) resulting in a

Table 5
DSC melting and cooling data of PFA samples.

Aging Time (h)	DSC-Heating		DSC-Cooling		X_c (%)
	T_m (°C)	ΔH_m	T_c (°C)	ΔH_c	
0	307.7	22.9	283.9	22.7	34.2
240	308.9	26.7	283.9	26.6	39.9
480	310.0	31.0	283.8	30.8	46.2
720	308.4	28.5	283.7	28.5	42.6
1000	307.8	27.4	283.6	25.8	40.9

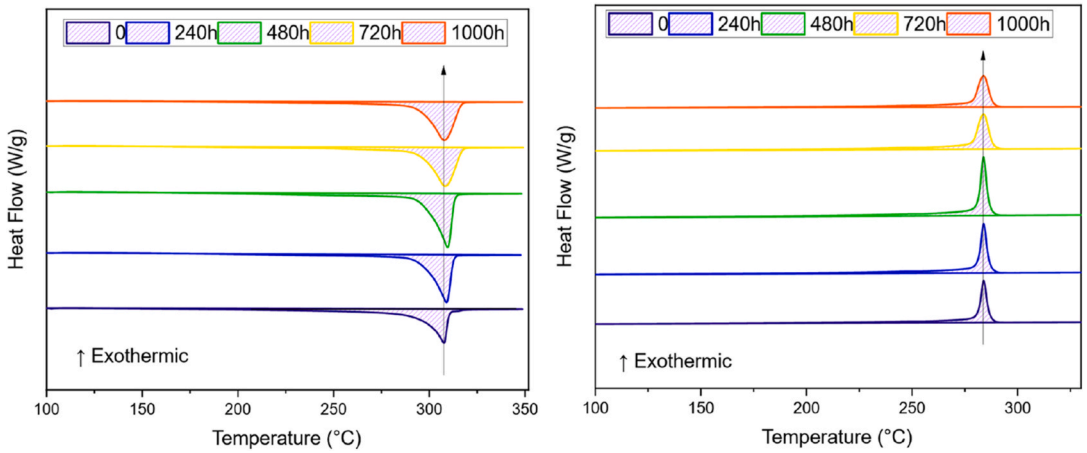

Fig. 7. DSC melting and cooling curves of PFA samples.

decrease in the crystallization ability of PFA as highlighted in weakening and broadening of DSC crystallization curve shown in Fig. 7. It can be noted that although aging affects the crystallization behavior of PFA but the crystallization temperature is not significantly influenced by the whole aging process.

3.5. Mechanical properties

Thermal oxidative aging impacts mechanical properties such as tensile strength and elongation at break of polymers. The effect of thermal aging on tensile strength and elongation at break of PFA is shown in Fig. 8(a and b). Stress and strain curve of PFA samples are presented in Fig. 8(c). The tensile strength of PFA films initially shows a slight increase during early stages of aging, rising from 18.5 MPa (at 0 h) to 18.8 MPa (at 240 h) and reaching a maximum of 19.8 MPa at 480 h. It should be noted that these values represent average measurements, and the observed increase up to 480 h remains within the standard deviation range, indicating only a marginal change in mechanical strength. This improvement reflects the physical aging and moderate chain scission that occur during the first stage of thermal exposure. Shortened polymer chains exhibit enhanced packing efficiency, which marginally increases crystallinity. These microstructural changes stiffen the amorphous phase and result in a marginal rise in tensile strength. Young modulus also shows a slight increase from 322 MPa to 330 MPa during the early aging stage. This trend is directionally consistent with the increase in crystallinity; however, the change in modulus is relatively small and should not be attributed to crystallinity alone. In semicrystalline polymers, the elastic modulus is influenced not only by crystalline fraction but also by lamellar organization, tie-molecule concentration, amorphous-phase mobility, and measurement variability. Therefore, the early increase in modulus is interpreted as a combined effect of moderate chemi-crystallization and local structural rearrangement, rather than a direct proportional response to the increase in the crystallinity. The results are consistent with previous research where the increase of crystallinity has increased hardness, reduced elongation at break and improved Young's Modulus of polyolefins and fluoropolymers [24,32,36,37]. The yield stress increases modestly up to 480 h of aging time as shown in Table 6, consistent with early crystallinity enhancement. Beyond 480 h, tensile strength decreases significantly to 16.6 MPa at 720 h and further to 10.7 MPa at 1000 h. The sharp decline marks the onset of oxidative degradation, where long-chain scission, carbonyl formation, and lamellar disruption weaken the structural integrity of the polymer. The yield stress also drops together with the elastic modulus which decease from 324 MPa at 720 h and further to 321 MPa at 1000 h as shown in Table 6, reflecting weakened amorphous domains and damaged initiation sites. These degradation processes reduce the effective load transfer between crystalline domains and the amorphous phase, leading to a reduction in stiffness.

Table 6
Tensile and DMA data of PFA samples.

Aging Time (h)	Tensile		Viscoelastic (DMA)	
	Young Modulus (MPa)	Yield Stress (MPa)	Storage Modulus at T_g (MPa)	T_g Peak (°C)
0	322	8.6	190.1	87.7
240	328	10.4	196.2	88.1
480	330	10.7	199.7	89.7
720	324	9.3	174.6	87.1
1000	321	8.5	160.1	85.2

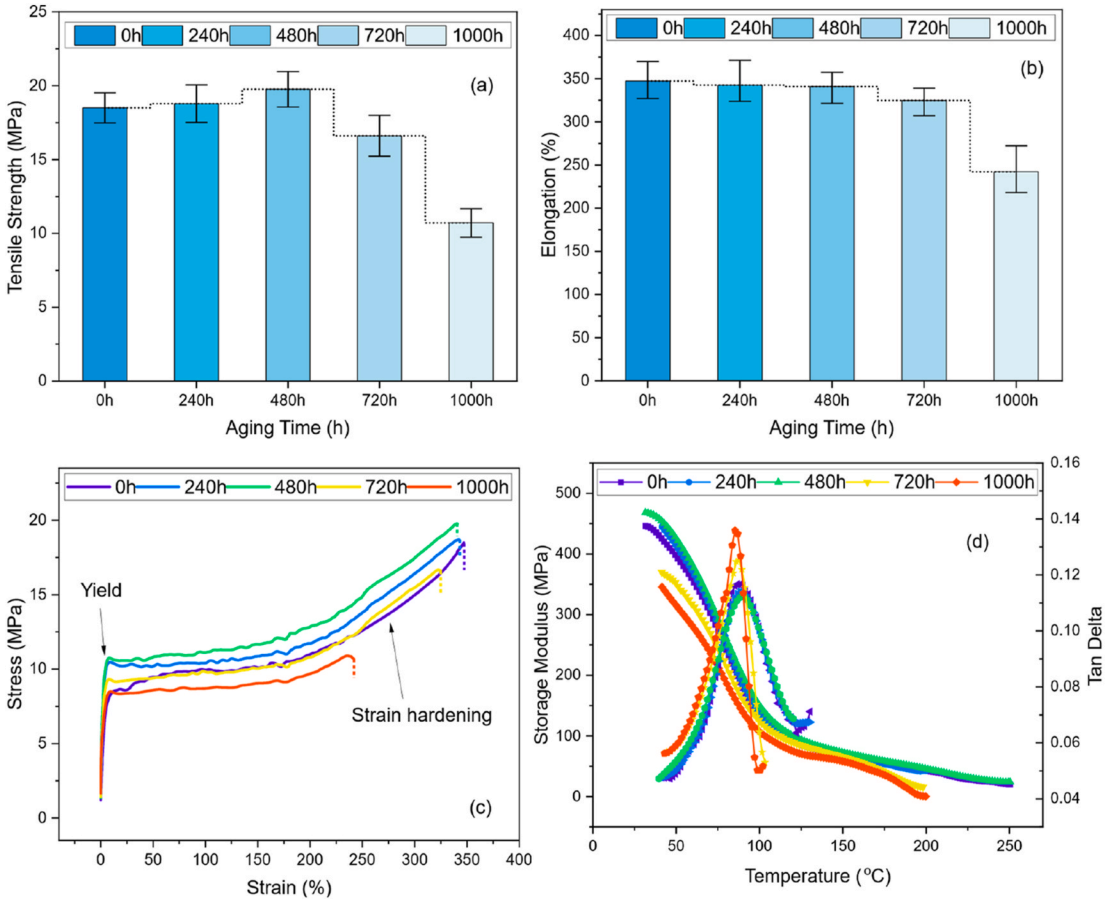

Fig. 8. Mechanical properties of PFA samples with aging time (a) tensile, (b) elongation (c) stress vs strain curves, (d) DMA (storage modulus and tan-delta).

Elongation at break follows a similar two-stage degradation pattern. Initially, elongation at break slightly decreases from 347% at 0 h to 342–340% at 240–480 h (Fig. 8(b)); however, the relatively large standard deviation suggests noticeable variability in ductility during this stage. This behavior is attributed to increased crystallinity (chemicrystallization), which reduces amorphous content (decreased interlamellar spacing) and limits chain mobility, as illustrated in Supplementary Fig. S7. However, PFA still retains substantial stretchability in this stage. A major deterioration occurs in the late stage, where elongation drops markedly to 324% (720 h) and further to 242% after 1000 h. This substantial reduction indicates the development of a brittle morphology, caused by oxidative cleavage, defect generation, and microvoid growth as illustrated in FTIR and SEM analysis. During elongation, polymer chains first uncoil, then align, then fully stretch. When the chains can no longer slide or extend, stress concentrates at weak, oxidized, shortened chain segments. The failure is caused by chain-level breakage due to these stress concentrates. The embrittlement in PFA at higher exposure time e.g. 720-1000 h may also occur due to decrease in the density of entanglements or tie-macromolecule concentration as illustrated in Supplementary Fig. S7 [38]. At higher stage of aging, severe chain scission results in chain fragments being too short to act as effective tie macromolecule. This leads to the destruction of tie-macromolecules network compromising the load transfer capability between the lamellae resulting in the collapse of strain-hardening and ductility. This phenomenon can be reflected from the decrease of slope of strain hardening region as shown in Fig. 8(c) as final failure point shifts to lower strains after 720–1000 h, confirming loss of structural integrity. The results clarify the transformation of PFA from a ductile (structurally stable polymer) to a brittle (oxidation-dominated system) limiting its ability to sustain high strains as illustrated in Supplementary Fig. S7.

The variation of DMA storage modulus (E′) and tanδ of PFA samples as a function of temperature is shown in Fig. 8 (d), respectively. Results in Table 6 indicates that the glass transition temperature (T_g) of PFA, defined as the temperature at the peak of tanδ, occurs at 87.7 °C, corresponding to (α) relaxation. The storage modulus for all PFA samples exhibits a gradual and progressive decline with increasing temperature, with a notable reduction observed in the temperature range of 70 °C-100 °C, corresponding to the PFA glass transition. This decrease in modulus is attributed to energy dissipation processes associated with the cooperative movements of polymer chains [39]. It is also evident from DMA results that the storage modulus of PFA shows a slight increase from 190.1 MPa (0 h) to 199.7 MPa with aging time (0-480 h) in the glass transition temperature region. The curves gradually converge and decrease at higher temperatures near and beyond T_g. The increase in storage modulus observed in this aging period unveils the increased load-carrying capacity and visco-elastic stiffness increasing mechanism of PFA polymer as observed in tensile analysis [40]. However, beyond 480 h the modulus decreases progressively, falling to 160.1 MPa at 1000 h. The decrease of E′ is more obvious, particularly at higher temperatures. The decline in storage modulus corresponds to the onset of oxidative chain scission, disruption of crystalline domains, increased free volume, and microstructural damage (as highlighted in Supplementary Figure S7). These changes provide indirect evidence of molecular weight reduction due to chain scission, as widely reported in the literature for fluoropolymers [8,20]. This leads to fewer entanglements and reduced stiffness, which lowers the storage modulus [8].

The tanδ of materials reflects the balance between the viscous and elastic phases in polymer-based systems. The tanδ (damping peak), typically observed in the glass transition region, is linked with the motion of side groups, low molecular weight units, or molecular chains in the polymer [8]. A higher damping peak indicates a higher molecular mobility [41]. It can be seen from Fig. 8 (d) that the tanδ peak (α-relaxation) of PFA diminishes and shifts forward towards higher temperatures (87.1 °C-89.7 °C) in early aging (0-480 h). The relaxation process is highly sensitive to molecular dynamics and the state of the amorphous regions. Early chain scission enhances the crystallinity (lamellae thickness I_c increases) as shown in Supplementary Fig. S7, which stiffens the amorphous regions of PFA (decrease interlamellar spacing I_a), and reduces the segmental motion of the amorphous chains, requiring more thermal energy to achieve the glass transition. With extension of aging time e.g. beyond 480 h, that the height of the tanδ peak increases and the peak position slightly shifts to lower temperatures (from 87.1 °C to 85.2 °C) in aging period (720-1000 h). Thermal oxidative aging dominates at a later stage of aging as highlighted in Supplementary Fig. S7 which results in severe chain scission phenomenon in PFA creating much shorter chains, polar groups and voids which facilitate segmental motion of polymer chains. The amorphous regions of polymer experience less restriction and molecular mobility is enhanced consequently. Shorter chains also require less thermal energy to achieve mobility, leading to a decrease in the temperature required for segmental motion (i.e., decrease in T_g). The increased storage modulus and reduced tanδ peak observed in early aging stage (0-480 h) of PFA indicate enhanced rigidity and reduced damping, making the PFA more resistant to deformation under mechanical stress. However, PFA loses its rigidity (reduced load-bearing capability) and becomes more brittle at later stage of aging (720-1000 h). The results of DMA are consistent with the tensile degradation analysis.

3.6. Dielectric analysis

Broadband dielectric spectroscopy was conducted over a frequency range of 10^{-1}-10^{6} Hz to assess changes in the dielectric behavior of PFA during thermal aging at 280 °C for up to 1000 h. The evolution of the dielectric constant (ε′) and dissipation factor (tanδ) provides insight into the molecular-level degradation processes and their influence on electrical functionality. The broadband dielectric spectroscopy (BDS) results of PFA are shown in Fig. 9. The unaged PFA exhibits a nearly frequency-independent dielectric constant of $\varepsilon' \approx 1.90$ across the entire 0.1–10^{6} Hz range as shown in Fig. 9(a), which is characteristic of fluoropolymers. This low and stable ε′ reflects the highly non-polar nature of the perfluorinated –CF_2–CF_2– backbone, limited orientational polarization, and restricted dipole mobility in the glassy–crystalline structure. It can be seen from Fig. 9(a) that the dielectric constant of PFA in nearly unchanged during at the early aging stage (0–480 h). The slight increase in dielectric constant can be attributed to enhanced interfacial (Maxwell–Wagner–Sillars) polarization occurring at the crystalline/amorphous phase boundaries inherent to the semicrystalline structure of PFA. These interfaces represent regions of contrast in molecular mobility and electrical conductivity, where charge carriers can accumulate. As the crystalline phase grows during early aging (chemicrystallization), the density of such interfaces increases, leading to a moderate enhancement of interfacial polarization and, consequently, a slight increase in ε′ [42,43]. However, the frequency dependency is minimal, suggesting that the primary dielectric relaxation processes are not strongly frequency-dependent in the range measured. As the aging process moves to the later stages (480-1000 h), dielectric polarization ability of PFA increases. The magnitude of the increase and the frequency dependance becomes more pronounced after 480 h (ε′ increases from 1.9 (0 h) to 2.15 (1000 h) at 0.1 Hz), marking the transition from a chemicrystallization-dominated regime to a degradation-dominated regime. Thermal aging at 280 °C for longer periods e.g. 1000 h promotes oxidative reactions in PFA, leading to the formation of oxygen-containing polar groups such as carbonyls, as discussed in FTIR analysis. These newly formed carbonyl-containing species introduce additional dipoles and significantly enhance the strength of relaxational polarization, resulting in a higher relative dielectric constant at low frequencies [44]. The increase in O/C ratio from EDS further supports this interpretation. Since relaxational polarization requires a finite response time, its contribution becomes increasingly suppressed as the electric field frequency rises. Consequently, aged PFA exhibits a pronounced increase in dielectric constant in the low-frequency region,

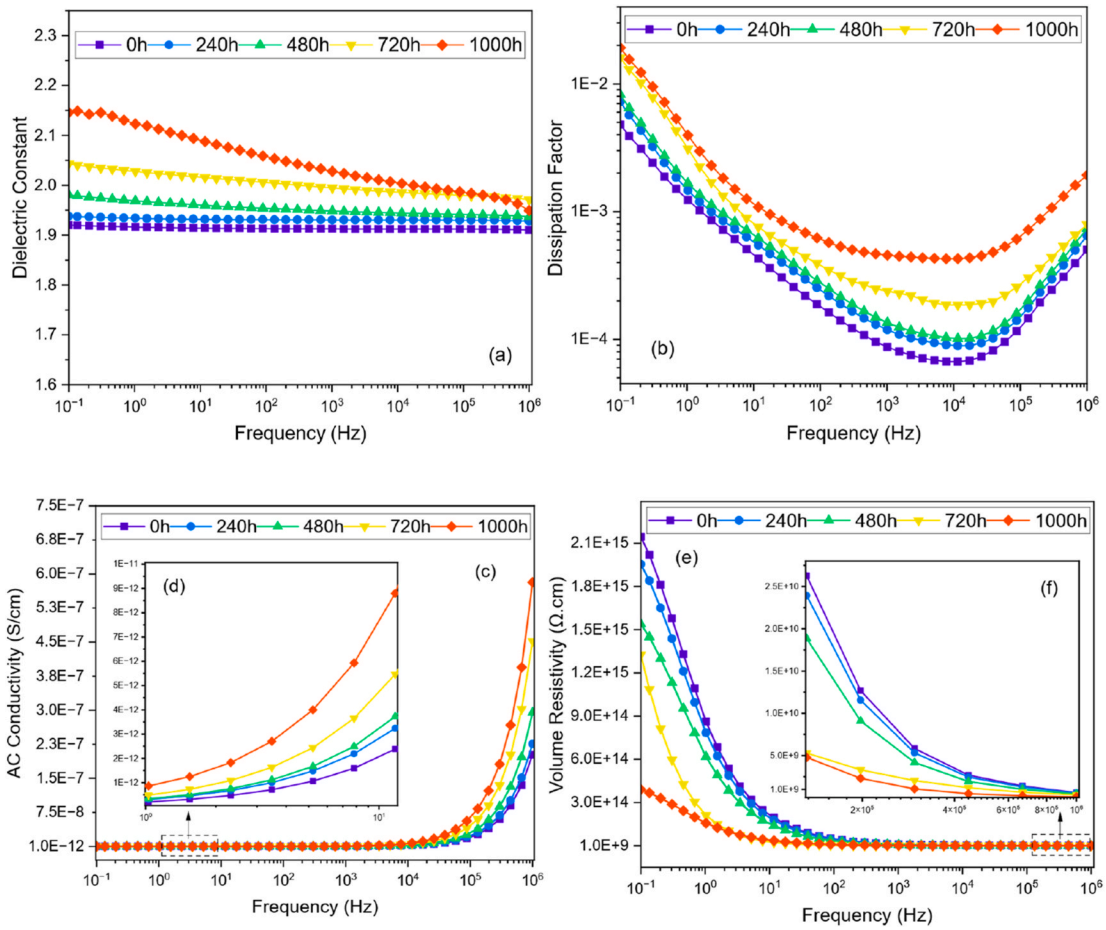

Fig. 9. Dielectric properties of PFA samples with aging time, (a) dielectric constant, (b) dissipation factor, (c-d) AC conductivity, (e-f) volume resistivity.

while the enhancement becomes much less significant at high frequencies where the newly formed dipoles cannot follow the rapidly oscillating electric field.

The unaged PFA displays extremely low dissipation factor (2.19×10^{-4} at 50 Hz), indicating minimal conduction and dipolar relaxation pathways. The dissipation factor increases with increase in aging time (0-1000 h) as shown in Fig. 9(b). The increase is not significant in early stage of aging (0-480 h). However, dissipation factor increases remarkably after 480 h reaching 6.84×10^{-4} at 1000 h. Dissipation factor in low frequency (10^{-2}-10^{2} Hz) and high frequency range (10^{4}-10^{10} Hz) is dominated by space charge along with DC conductivity and dipole relaxation polarization phenomenon respectively [45,46]. The conductivity loss related to space charge polarization is enhanced particularly at low frequencies which increases dissipation factor in PFA. Thermal oxidative degradation becomes dominant at the later stage of aging (480-1000 h) which changes the molecular dynamics of PFA, disrupts the crystalline zone of PFA and breaks tier macromolecular chains (increased localized mobility as reflected by DMA) thus enabling energy dissipation through dipolar motion. Prolonged exposure to high temperatures for long term (e.g. 1000 h) also results in generation of more polar and reactive functional groups and pyrolysis degradation by-products [9]. This trend correlates closely with the FTIR spectra, which show a sharp increase in carbonyl index in the later aging stage, highlighting the formation of carbonyl-containing and other oxygenated functional groups. These species are responsible for enhancing the relaxation polarization mechanism in PFA thus increasing energy dissipation in high frequency range (10^{4}-10^{6} Hz). Moreover, Cleavage of C–F and C–O bonds can produce reactive intermediates such as acyl fluoride (–COF), carbonyl-containing species, and unsaturated groups (–CF=CF–). Some of these fragments may subsequently undergo secondary reactions or partial ionization, forming charged species such as fluoride-containing fragments or oxidized fluorocarbon species. These charged or partially ionic degradation products can migrate within the amorphous phase under an applied electric field, contributing to the density of trapped changes (space-charge accumulation) and increased electrical conductivity as shown in Fig. 9(c and d). These polar groups are also conductive to charge carrier movement which reduces the volume resistivity of PFA significantly as shown in Fig. 9(e and f) [47]. The volume resistivity at low frequency e.g. at 0.1 Hz decreases significantly from 2.14×10^{15} Ω cm (0 h) to 3.90×10^{14} Ω cm (1000 h), indicating enhanced charge transport with aging. A similar decreasing trend is observed in the high-frequency region, as highlighted in Fig. 9 (f).

To further analyze the conduction mechanism of PFA, the AC conductivity spectra were fitted using the Almond–West formalism, as shown in Fig. 10(a) and results are given in Table 7. The frequency dependence of conductivity for the aged and unaged PFA samples follows the Almond–West expression, which can be written as [48]:

$$\sigma(\omega) = \sigma_{DC}\left[1 + \left(\frac{\omega}{\omega_c}\right)^{n}\right] \quad (3)$$

where σ_{DC} is the DC conductivity, n is the power-law exponent describing the electrical relaxation behavior (typically $0.5 \leq n \leq 1$) [49], and ω_c represents the characteristic hopping frequency of charge carriers. The parameter ω_c defines the transition from the low-frequency DC plateau to the high-frequency dispersive region where hopping conduction dominates ($\omega \geq \omega_c$).

The results in Table 7 show that the DC conductivity of PFA increases

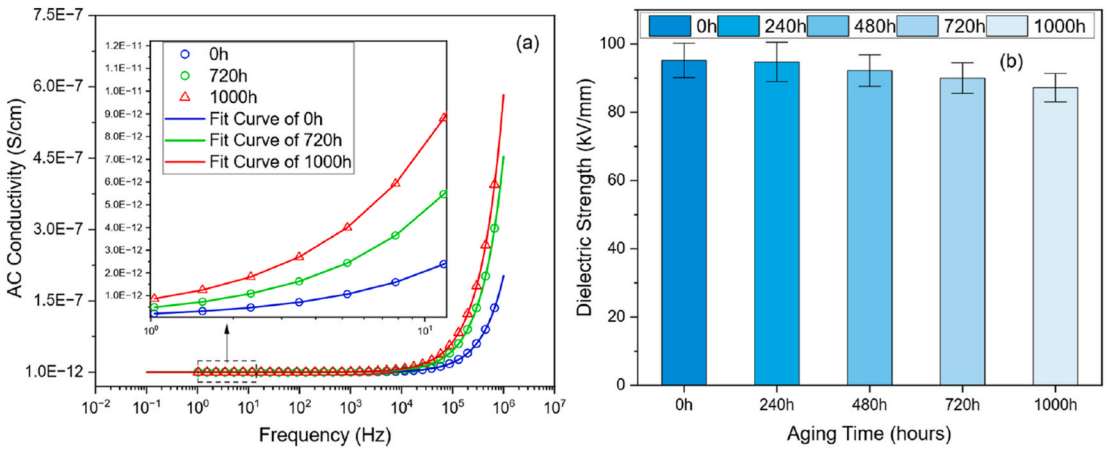

Fig. 10. (a) Almond West formalism AC conductivity curve fitting, (b) Dielectric strength.

Table 7
Almond West AC conductivity curve fitting data.

Samples	0 h	720 h	1000 h
σ_{DC} (x10^{-12} S/cm)	1.58	3.75	7.70
f_c (Hz)	7.75	7.97	8.57
n	0.999	0.996	0.962
τ (s)	0.020	0.019	0.018
Adj. R^2 (%)	99.98	99.99	99.98

significantly in thermal aging period (720-1000h). The overall rise in conductivity ($\sigma \propto n_c u$) of PFA is attributed to the formation of oxygen-containing polar groups during degradation, which increases both the charge carrier density (n_c) and mobility (u). The characteristic crossover frequency (ω_c) also shifts to higher values in aged PFA samples, indicating faster charge-carrier dynamics. Thermal exposure at 280 °C for longer periods e.g. 720-1000 h can promote extensive chain scission in PFA, increasing segmental mobility in the amorphous phase as discussed earlier. This enhanced molecular mobility reduces the relaxation time ($\tau = 1/2\pi f_c$), causing ω_c to move toward higher frequencies, consistent with the trend summarized in Table 7 [50].

The variation of dielectric strength of PFA with aging time is shown in Fig. 10(b). It can be seen from the results that the dielectric strength of PFA decreases with aging time. The decrease is not significant at the early stages of aging. However, a noticeable reduction of 8.4% in dielectric strength is observed when PFA is exposed to high temperatures for longer periods e.g. 1000 h. The destruction of PFA lamellae due to thermal oxidative stress could be the reason for the decrease in dielectric strength. Molecular density is reduced resulting in increased free volume and mean free path for charge carriers. These changes make the charge carrier migration easier between the crystalline and amorphous zones facilitating the electron impact ionization phenomenon [8, 44]. As discussed previously, severe aging can also result in generation of reactive polar groups which can also contribute to the traps and trap charges in PFA. As a result, the charge injection becomes easier in dielectric medium. Consequently, the dielectric integrity is affected, and the dielectric strength is reduced.

To understand whether the reduction in dielectric strength of PFA during thermal aging originates from mechanical degradation or dielectric polarization changes, the Stark–Garton relation was applied [25]. The model reveals how stiffness changes and polarity changes jointly affect dielectric strength. In this model, the mechanical breakdown field E_M is expressed as:

$$E_M \propto \sqrt{\frac{Y}{\varepsilon}} \tag{4}$$

where Y is Young's modulus and ε is the dielectric constant. To directly compare model-predicted breakdown field E_M and measured dielectric strength E_D, both E_M and E_D were normalized to their unaged (0h) values (E_{M_0} and E_{D_0}) and the results are listed in Table 8.

In the early stage of aging (0-480 h), the Young's modulus increases slightly due to chemicrystallization, while the dielectric constant increases only marginally from 1.90 to 1.98. As a result, the ratio Y/ε remains nearly constant, and the model predicts only a negligible reduction in the mechanical breakdown field (normalized E_M/E_{M0} = 1.00→0.99). This agrees well with the measured dielectric strength, which remains almost unchanged in this period (95.2 → 92.2 kV/mm). At longer aging times (480-1000 h), however, oxidative chain scission becomes dominant, reducing the modulus and simultaneously increasing the dielectric constant (from 1.98 to 2.15) due to the formation of polar degradation products and microvoids. Consequently, Y/ε decreases sharply, and the predicted dielectric strength drops to 0.94 of its initial value, closely matching the experimental decline to 87.1 kV/mm. The correlation between the measured dielectric strength and the modelled $\sqrt{Y/\varepsilon}$ relationship confirms that the loss of dielectric strength in aged PFA is governed primarily by the combined effect of mechanical softening (reduced stiffness due lamellar degradation) and the increase in dielectric constant (polar group formation) arising from oxidation-induced chain scission.

3.7. *Effect of temperature on PFA microstructure (using MDS)*

The variation of the calculated free volume of PFA at different temperatures is shown in Figs. 11 and 12 (c). It can be seen from the results in Table 9 that the percentage of free volume of PFA increases gradually with the increases of temperature reaching a maximum of 31052.55 Å3 at 300 °C. When the temperature increases, the molecular thermal motion mechanism of PFA dominates in the amorphous region, and the thermal energy input is converted into kinetic energy of molecular chains (especially amorphous segments), intensifying the thermal motion (vibration, rotation, and transition) of the segments, resulting in an increase in the average distance between molecules,

Table 8
Stark–Garton analysis for dielectric strength.

Aging Time (h)	Normalized Model Prediction (E_M/E_{M_0})	Normalized Dielectric Strength (E_D/E_{D_0})	Dielectric Strength (E_D) (kV/mm)
0	1.000	1.000	95.2
240	1.001	0.996	94.8
480	0.992	0.968	92.2
720	0.966	0.945	90.0
1000	0.939	0.915	87.1

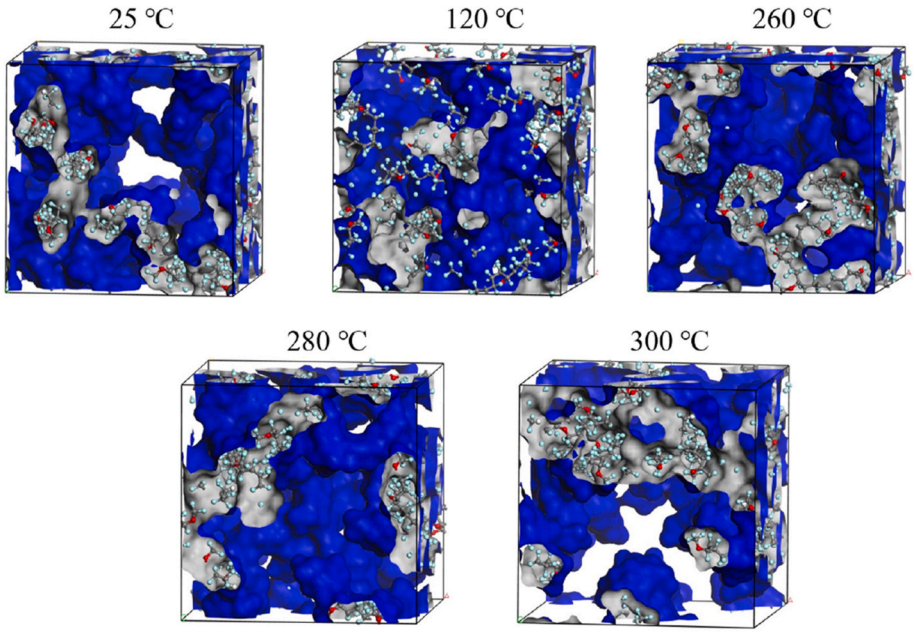

Fig. 11. Variation of free volume of PFA with temperature.

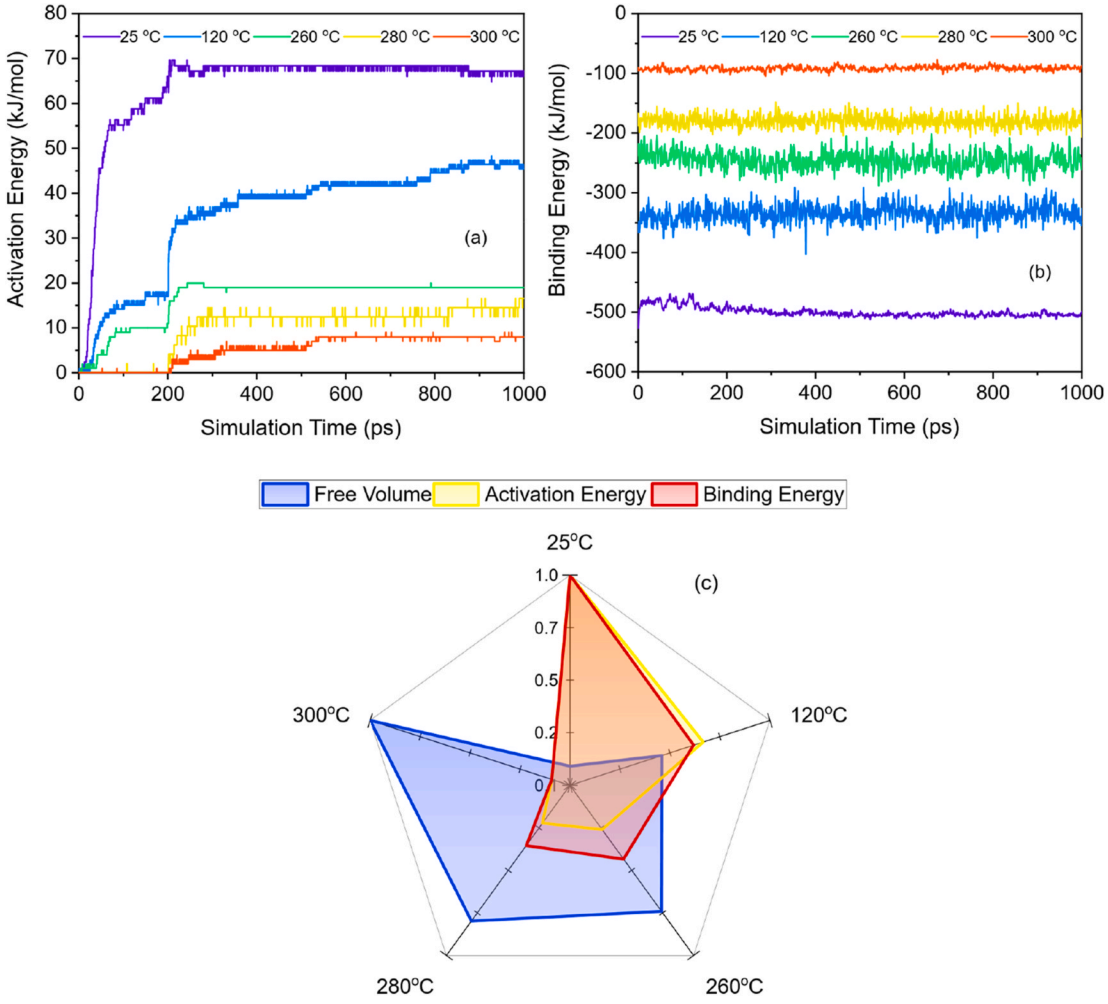

Fig. 12. (a-b) Convergence of binding and activation energy, (c) variation of free volume, activation energy and binding energy of PFA with temperature.

thereby creating and expanding unoccupied space. This phenomenon can be correlated with the aging of PFA at high temperature where long

Table 9
Free volume, binding energy and activation energy of PFA at different temperature.

Properties	Temperature				
	25 °C	120 °C	260 °C	280 °C	300 °C
Free Volume (Å^3)	18364.4	23524.0	27426.8	28236.3	31052.5
Activation Energy (kJ/mol)	67.2	45.4	19.0	16.6	8.0
Binding Energy (kJ/mol)	498.8	326.2	242.2	206.4	87.0

term exposure to high temperatures above the service temperature of polymer destroys the crystal structure of polymer resulting in an increased free volume [44].

It can be observed from the results in Fig. 12(a and b) that the activation energy and binding energy gradually converges and stabilizes with the increase of simulation time for all temperature models, which indicates that the PFA molecular structure reaches a decent stable state. The values of activation energy and binding energy reported in Table 9 are taken from the final equilibrated region (950-1000 ps) of simulation and are presented as absolute magnitudes. Molecular dynamics simulations show that the thermal degradation of PFA is governed by a competitive network of parallel reaction pathways, each possessing distinct activation energies. At lower temperatures, the slower reaction pathway that requires high activation energy becomes the "rate determining step" (rate control step). As the temperature increases, the apparent behavior of the entire reaction becomes increasingly dominated by (chain breakage and "zipper opening" reaction) processes that are more prone to occur (low activation energy pathway). The main chain of PFA molecules is a strong C-C bond, and the side chains include C-O bonds. When the temperature is very high (such as approaching or exceeding its melting point, about 300 °C as shown in Fig. 12 (c)), molecular thermal motion is extremely intense. Although C-C bonds themselves are strong, extremely high thermal energy is sufficient to directly cause them to undergo homolysis and generate free radicals [19,33]. Once this process begins, it may trigger a chain reaction. A defect at one end of a chain (such as - COOH or - COF) can trigger adjacent C-C bond cleavage under thermal energy, releasing monomers or small molecular fragments (such as tetrafluoroethylene, perfluoropropyl vinyl ether). Then, the defect at the end of the fracture can continue to trigger the breakage of the next key, like a "zipper" quickly unraveling a long molecular chain [33]. At high temperatures (280-300 °C), these low activation energy "zipper breaking" processes and direct fracture processes become very rapid, becoming the main contributors to degradation. Therefore, the activation energy calculated from macroscopic dynamic data shows a decreasing trend as shown in Table 9. This mechanistic picture is consistent with the experimental aging behavior observed during long-term exposure of PFA at 280 °C. Early-stage property changes are mild, but at later stages (720-1000 h), accelerated chain scission and zipper degradation dominate, leading to severe reductions in tensile strength, elongation, thermal stability, crystallinity, and dielectric dielectric strength.

The binding energy is the 'effective binding energy' required to maintain the overall structural stability and integrity of a material. It reflects the material ability to resist external forces such as peeling, wear, and deformation. In the context of PFA aging, the increase in molecular thermal motion due to temperature is a key factor in the breakdown of intermolecular forces, specifically van der Waals forces that maintain the polymer structure. As temperature increases (such as during thermal aging at 280 °C), the kinetic energy of PFA long molecular chains increases, resulting in increased vibration and motion of the polymer segments. This leads to stretched intermolecular distances, reducing the attraction between chains and thus weakening the material structure at the microscopic level. PFA, being a semi-crystalline polymer, contains both crystalline and amorphous regions. The crystalline regions act as "anchor points", providing strength and stability, while the amorphous regions offer flexibility as previously illustrated in Supplementary Figure S7. As temperature increases, especially near melting point (T_m) (as shown in Fig. 12(c)),the molecular segments in the amorphous region first gain sufficient energy, and become free to move from a frozen state, causing the material to soften. More importantly, thermal energy can also destroy the lattice at the edges of the crystalline region (as shown in Supplementary Fig. S7) that is not perfectly arranged. The thermal motion of molecular chains makes it easier for them to "break free" from the lattice, resulting in a decrease in overall crystallinity. The decrease in crystallinity means a reduction in the number of strong "anchor points" and a significant weakening of the effective binding of the entire polymer network as shown in Table 9. The material transitions from a rigid and tough state to a viscoelastic state. Macroscopic manifestations at this stage include decreased modulus and strength. This is confirmed by experimental results, where changes in crystallinity (increasing initially, then decreasing at later stages) and significant decreases in tensile strength and elongation (due to the weakening of the crystalline structure and softening of the amorphous regions) were observed.

3.8. Discussion

The aging behavior of PFA insulation material was studied under thermal oxidative conditions at 280 °C, a temperature commonly encountered in high-voltage cable systems in aerospace applications. The degradation process in PFA occurs in distinct stages, each impacting its mechanical, dielectric, and structural properties. As shown in the aging mechanism diagram in Fig. 13, the initial degradation of PFA is dominated by thermal chain scission at elevated temperatures.

During the first 480 h, the degradation mechanism primarily involves the random chain scission process and chemicrystallization, leading to an increase in crystallinity and slight enhancement in mechanical properties. Early to mid-chain scission results in a decrease in molecular mass and slight formation of polar groups. These changes are reflected in the dissipation factor curve shown in Fig. 14, which increases gradually from 2.19×10^{-4} (at 0 h) to 3.36×10^{-4} (at 480 h). The elongation retention also remains relatively stable, with a slight decrease from 100% to 98.6%. This period can be considered as the “healthy region”, where the material retains most of its mechanical and dielectric properties. In this stage, the PFA material is still operationally sound, maintaining sufficient mechanical and dielectric strength, which is crucial for high-voltage cable performance.

After 480 h, the material enters a transition phase where oxidation reactions begin to dominate due to oxygen diffusion into the polymer matrix. As seen in the dissipation factor curve shown in Fig. 14, there is a noticeable increase in dissipation factor from 3.36×10^{-4} (480 h) to 4.42×10^{-4} (720 h) crossing the EOL point (EOL-100% increase in dissipation factor). This increase is indicative of the oxidative degradation of the polymer, leading to the formation of polar groups that elevate the dielectric constant as illustrated in Fig. 13. The elongation retention also starts to decline more rapidly, decreasing from 98.1% at 480 h to 93.5% at 720 h. This behavior suggests the onset of material softening and loss of structural integrity. The material enters the “wear-out region”, where performance begins to degrade significantly, but it is still useable for a limited period as PFA has not reached the conversative EOL1 (70% retention point in elongation).

In the final stages of aging, after 720 h, the dissipation factor continues to rise dramatically, reaching 6.84×10^{-4} at 1000 h, signaling severe degradation. The elongation retention also drastically drops to 69.7% crossing EOL1, indicating a significant loss in mechanical strength and flexibility. This is marked as “disposal or unhealthy region” in Figs. 14 and 15, where PFA can no longer maintain reliable mechanical or dielectric properties. It can be noted from Fig. 14 that the PFA after 1000 h has not crossed the traditional EOL2 criterion (50% elongation retention), which is commonly adopted as an end-of-life

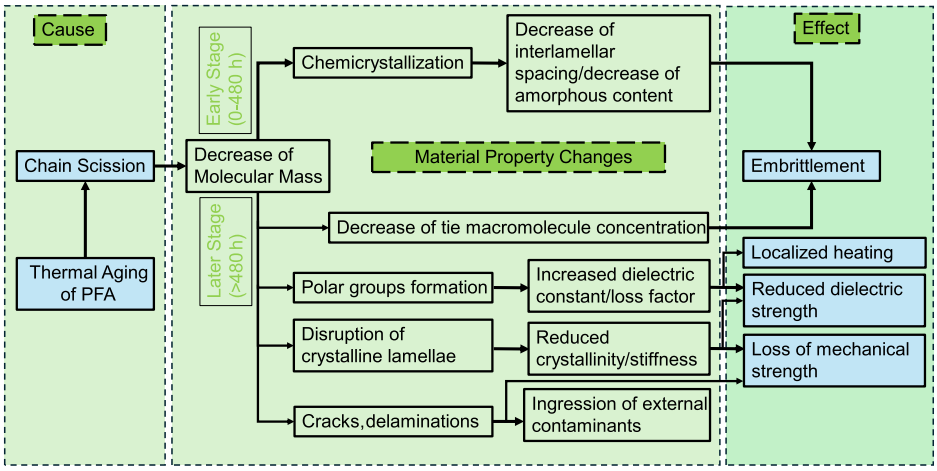

Fig. 13. Degradation mechanisms in PFA under thermal oxidative stress.

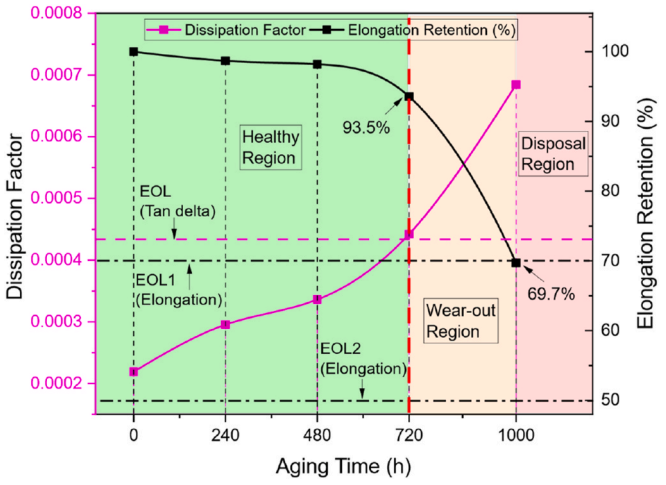

Fig. 14. Elongation retention (%) and dissipation factor of PFA (at 50 Hz) with aging time.

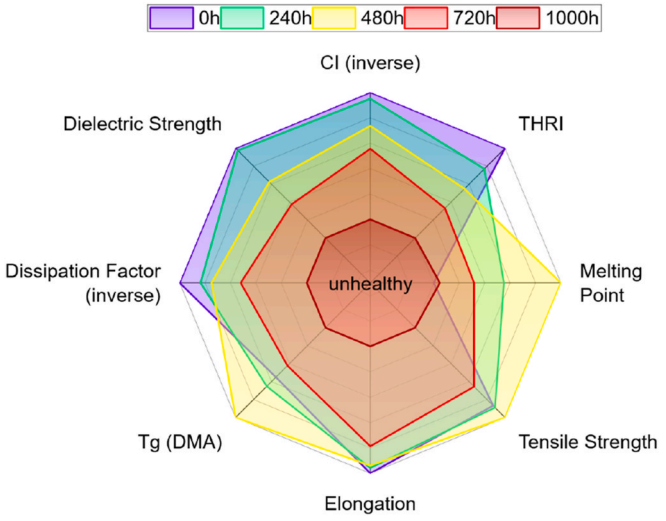

Fig. 15. Performance radar chart of PFA.

indicator for polymeric insulation materials in high-voltage cable applications [23]. As shown in the performance radar chart in Fig. 15, key properties such as tensile strength, dielectric properties, and Tg (DMA) decline significantly in the unhealthy region. The material has surpassed its operational limit and continuing to use it in this state could lead to catastrophic failures, especially in high-voltage cable applications. This degradation is directly related to the disruption of crystalline lamellae, decrease in tie macromolecule concentration, and the increase in dissipation factor and permitivity due to polar functional groups. For high-voltage cables, a higher dielectric constant distorts the electric field distribution and increases the likelihood of partial discharge, while elevated dissipation factor generates additional Joule heating as highlighted in Fig. 13 [44]. Without adequate thermal management or enhanced thermal conductivity in cable design, this localized heat accumulation raises the internal temperature of the cable and accelerates insulation aging. Such coupled electrical-thermal degradation ultimately compromises the primary insulation and shortens the operational lifetime of onboard high-voltage cables. Considering real service temperatures of onboard HV cables (200 °C and 240 °C for short time e.g. 15 min during power surge), the aging process would occur slower compared to 280 °C. At these temperatures, the PFA material will exhibit prolonged useful life, as lower temperatures reduce the degradation rate as reflected in MDS results. Therefore, in real service environments, PFA can be expected to perform reliably for approximately 500-1000 h at temperatures between 200 °C and 260 °C, before entering the wear-out region.

Crack formation observed in PFA can also affect the degradation process as shown in Fig. 13. During the manufacturing of polymeric cable insulation, microscopic voids and interfacial defects are inevitably introduced into the insulation. Under electrical stress, these defects act as local electric-field enhancers. For a spherical void embedded in a dielectric medium with dielectric constant of ε_r, the electric field inside the void is amplified by a factor K [1]:

$$K = \frac{3\varepsilon_r}{1 + 2\varepsilon_r} \tag{5}$$

Partial discharge (PD) inception occurs when the product of the local electric field in void and the void thickness t_v exceeds the breakdown voltage of air in void. According to the single void discharge (SVD) method, the required insulation thickness t_i follows an exponential relationship with applied voltage V, void size t_v, and shape factor K, given by Ref. [51]:

$$t_i = r_c\left(\exp\left(\frac{KVt_v}{\alpha r_c}\right) - 1\right) + C \tag{6}$$

where r_c is the conductor radius, C is a constant and α is the minimum breakdown voltage of air in the cavity e.g. 250 V [51,52]. This relationship highlights the strong sensitivity of insulation reliability to small

increases in void size and dielectric constant. As mentioned previously, long term exposure to high temperature e.g. (for 1000 h) induces molecular chain scission and oxidative degradation in PFA, leading to the formation of polar functional groups such as carbonyl groups which increase the dielectric constant, thereby increasing the field enhancement factor K. Simultaneously, SEM observations revealed the development of micron-scale surface cracks, which may increase the equivalent void size t_v. The combined increase in K and t_v will lower the PD inception threshold, increasing the likelihood of partial discharge activity under normal operating voltages. Furthermore, aging induced surface cracks in PFA can also facilitate penetration of external contaminants e.g. moisture as highlighted in Fig. 13, which may further enhance polarization and dissipation factor and can promote charge accumulation at defect interfaces, further accelerating dielectric degradation. Although PFA is hydrophobic in nature, but it cannot withstand water absorption as good as PTFE [7]. At a later stage of aging e.g. 1000 h, the use of PFA with the presence of surface cracks and prevailing humid aerospace environmental conditions (RH~85%) can be cautious for insulation integrity of onboard cables. Although increasing insulation thickness could mitigate risk, such an approach is impractical for aircraft cable systems due to strict mass and volume constraints. In contrast, the current use of multilayer aerospace cable architecture incorporates semiconductive shielding layers and multiple interfaces which can provide effective electric-field grading and environmental protection and therefore limit the crack-driven degradation in PFA insulation thereby aiding to the reliability. As the overall reliability of onboard HV cables depends on the degradation behavior of all layers rather than the bulk dielectric alone, so future evaluations of aircraft HV cable performance should therefore assess the aging characteristics of both the insulation material and the semiconductive shielding materials, along with their interfacial stability.

3.9. Health, safety, and handling considerations of PFA

PFA is widely regarded as a chemically inert and stable fluoropolymer under normal service conditions, which supports its extensive use in high-performance electrical insulation. However, under elevated temperatures, particularly during thermal degradation or processing above its service range, PFA can release small amounts of decomposition products, including fluorinated compounds and trace quantities of hydrogen fluoride (HF), carbonyl fluoride (COF_2), and perfluoroisobutylene (PFIB) [28,53]. Although the quantities released are generally low, these species may pose potential health risks if adequate precautions are not taken.

In addition, PFA may react with highly reactive substances such as halogenated fluorine compounds (e.g., ClF_3, BrF_3), alkali metals (e.g., sodium, potassium), and certain metal hydrides at elevated temperatures. Mixtures of finely divided fluoropolymers with reactive metals (e.g., aluminum or magnesium) may also present flammability or explosion hazards under specific conditions [28].

During high-temperature treatments, including thermal aging experiments, appropriate safety measures are essential. Experimental setups should be operated in well-ventilated environments, with ovens connected to exhaust hoods to ensure proper removal of any evolved gases [53]. Direct exposure to hot vapors should be avoided, and it is recommended not to open the oven at elevated temperatures (e.g., 280 °C), as this may result in sudden release of fluorinated fumes. In our experimental observations, such conditions were sufficient to trigger sensitive smoke detection systems, highlighting the presence of otherwise invisible gaseous by-products.

Personal protective equipment (PPE), including safety glasses and heat-resistant gloves, should be used when handling PFA, especially at high temperatures. Inhalation of decomposition fumes or contaminated smoke (e.g., from tobacco exposure) should be strictly avoided, as it may lead to temporary flu-like symptoms (polymer fume fever) [28,53]. In case of contact with molten material, appropriate first-aid procedures should be followed.

Overall, while PFA remains safe and stable under normal operating conditions, understanding its high-temperature decomposition behavior is important not only for material performance but also for ensuring safe handling and operation in laboratory and industrial environments.

4. Conclusions

This study provides a comprehensive evaluation of the thermal aging behavior of PFA as an insulation material for high-voltage cables used in aerospace applications. The results obtained from a wide range of experimental techniques, chemical analysis (FTIR), SEM/EDS, TGA/DSC, mechanical tensile tests, DMA, and dielectric measurements reveal the complex degradation mechanisms that drive the performance changes of PFA at elevated temperatures.

1. Chemical analysis in (FTIR) confirmed the formation of polar groups and oxidation as primary degradation processes, supported by SEM/EDS images, which showed evidence of crack formation and oxidative damage on the material surface with prolonged aging.
2. TGA/DSC results indicated a reduction in thermal stability with aging, along with shifts in the melting and crystallization behavior. Initially, at lower aging times (0-480 h), PFA exhibited increase in crystallinity. Expoure to high temperature for longer periods e.g. (720-1000 h) distrupted the crsytalline phase which is indicative of reduction of crystallinity and a loss of structural integrity.
3. Mechanical testing, including tensile strength and elongation at break, showed a significant decline after 720 h of aging, signaling embrittlement and material softening due to chain scission and the reduction of molecular mass. These findings were corroborated by DMA analysis, where decreased Tg confirmed the loss of molecular rigidity and flexibility at high exposure time e.g. 720-1000 h.
4. Dielectric properties, including dissipation factor and dielectric constant, exhibited an increase as aging progressed, further supporting the occurrence of oxidative degradation and the formation of polar groups. The dielectric strength of PFA decreased noticeably after prolonged thermal exposure e.g. 1000 h.
5. In addition to experimental methods, MDS were employed to explore the underlying degradation mechanisms at the molecular level. The simulations revealed that PFA degradation is driven by a competitive network of reaction pathways with different activation energies. The MDS confirms the chain scission and "zipper opening" reactions that predominate at high temperature, leading to lower activation energies and faster degradation. These simulation results are consistent with the experimental observations of structural weakening and performance loss over time.

This study concludes that PFA insulation can remain operational for up to 720 h at 280 °C, after which it enters the wear-out region. The 70% retention of elongation and 100% increase in dissipation factor can serve as end-of-life (EOL) criteria for PFA.

The comprehensive results from both experimental testing and MDS simulations offer valuable insights into the thermal aging of PFA and underscore the importance of considering chemical stability, mechanical integrity, and dielectric properties in the selection of insulation materials for high-voltage aerospace cables. While the present study focuses on thermal oxidative aging as a dominant degradation factor, aircraft cables in service are subjected to coupled electro-thermal-mechanical stresses. Therefore, future work will include aging studies on full-scale aircraft high-voltage cables, enabling evaluation of the degradation behavior of both the insulation material and the semiconductive shielding layers, as well as their interfacial stability under coupled operating conditions.

CRediT authorship contribution statement

Jawad Ahmad: Conceptualization, Data curation, Formal analysis, Investigation, Methodology, Visualization, Writing – original draft, Writing – review & editing. **Mohamad Ghaffarian Niasar:** Conceptualization, Funding acquisition, Project administration, Supervision, Writing – review & editing.

Declaration of competing interest

The authors declare that they have no known competing financial interests or personal relationships that could have appeared to influence the work reported in this paper.

Acknowledgement

This project is funded by the Dutch Nationaal Groeifonds (NGF) program Luchtvaart in Transitie, project STD1 Elektrische Kabelsystemen (grant no. 31194660), which is gratefully acknowledged. Authors also highly acknowledge the Delft Aerospace Structures and Materials Laboratory of the Faculty of Aerospace Engineering of TU Delft for the provision of research facilities.

Appendix A. Supplementary data

Supplementary data to this article can be found online at https://doi.org/10.1016/j.polymertesting.2026.109181.

Data availability

Data will be made available on request.

References

[1] R. Guo, J. Dong, R.E. Wolleswinkel, R. de Vries, M.G. Niasar, Electrical architecture of 90-Seater electric aircraft: a cable perspective, IEEE Trans. Transp. Electrif. 11 (2) (2025) 6854–6865.
[2] M. Borghei, M. Ghassemi, Insulation materials and systems for More- and all-electric aircraft: a review identifying challenges and future research needs, IEEE Trans. Transp. Electrif. 7 (2021) 1930–1953.
[3] "*ASD-STAN*" – Aerospace Series Cable Code Identification List.
[4] Zhengdong Wang, et al., Enhancing electrical insulation and thermal conductivity in polymer through constructing energy-dissipation organic electron acceptor/inorganic filler, Small 21 (22) (2025) 2502696.
[5] Meng Luo, et al., Enhanced dielectric breakdown strength and thermal conductivity of silicone gel composites with high-electron-affinity silicon dioxide/cationic Polymer/nano-Diamond, Chem. Eng. J. 501 (2024) 157623.
[6] B. Gilmore, Z. Luscher, K. Roberts, G. Fisher, T.D. Sparks, Comparison of fatigue in fiber-backed PVDF and PFA fluoropolymer linings, Polym. Degrad. Stabil. 162 (2019) 122–128.
[7] G. Lopez, High-performance polymers for aeronautic wires insulation: current uses and future prospects, Recent Prog. Mater. 3 (1) (2021) 1–15.
[8] Jawad Ahmad, Mohamad Ghaffarian Niasar, Aging behavior of PEEK, PTFE, and PI insulation materials under thermal oxidative and humid conditions for aerospace applications, J. Appl. Polym. Sci. 142 (19) (2025) e56858.
[9] Younnes Chikhoune, et al., Thermal ageing of an extrudable fluorinated polymer for aerospace application, in: 2024 IEEE 5th International Conference on Dielectrics (ICD), IEEE, 2024.
[10] Weijun Yin, Patricia Irwin, Daniel Schweickart, Dielectric breakdown of polymeric insulations aged at high temperatures, in: 2008 IEEE International Power Modulators and High-Voltage Conference, IEEE, 2008.
[11] L. Monson, Sung In Moon, C.W. Extrand, Gas permeation resistance of various grades of perfluoroalkoxy–polytetrafluoroethylene copolymers, J. Appl. Polym. Sci. 111 (1) (2009) 141–147.
[12] Geng Fei, et al., Radiolytic preparation of PFA-g-PVBSA membranes as a polymer electrolyte membrane, Nucl. Instrum. Methods Phys. Res. Sect. B Beam Interact. Mater. Atoms 274 (2012) 83–86.
[13] Gilbert Legeay, et al., AF fluoropolymer for optical use: spectroscopic and surface energystudies; comparison with other fluoropolymers, Eur. Polym. J. 34 (10) (1998) 1457–1465.
[14] S. Perelygin, M.Z. Peskova, Z.Z. Zakirov, I.M. Glikin, Determination of the crystallinity of polytetrafluoroethylene from infrared absorption spectra, J. Appl. Spectrosc. 24 (1976) 732–734.
[15] X. Huang, J. Martinez-Vega, D. Malec, Morphological evolution of polytetrafluoroethylene (PTFE) during thermal-oxidative ageing above and below the melting temperature, in: 2013 IEEE International Conference on Solid Dielectrics (ICSD), IEEE, 2013, pp. 628–631.
[16] A. Frick, D. Sich, G. Heinrich, D. Lehmann, U. Gohs, C. Stern, Properties of melt processable PTFE/PEEK blends: the effect of reactive compatibilization using electron beam irradiated melt processable PTFE, J. Appl. Polym. Sci. 128 (2013) 1815–1827.
[17] MeiJun Zhou, et al., Effects of molecular structure and temperature field on the crystallization behavior of poly (tetrafluoroethylene-co-perfluoroalkylvinyl ether), Polymer 311 (2024) 127508.
[18] A.M.S. Galante, O.L. Galante, L.L. Campos, Study on application of PTFE, FEP and PFA fluoropolymers on radiation dosimetry, Nucl. Instrum. Methods Phys. Res. Sect. A Accel. Spectrom. Detect. Assoc. Equip. 619 (1–3) (2010) 177–180.
[19] U.H. Hossain, F. Muench, W. Ensinger, A comparative study on degradation characteristics of fluoropolymers irradiated by high energy heavy ions, RSC Adv. 4 (91) (2014) 50171–50179.
[20] X. Huang, J. Martinez-Vega, D. Malec, Dielectric breakdown and morphological evolution of PTFE during thermal-oxidative ageing at temperatures lower and higher than the melting temperature, in: 2013 Annual Report Conference on Electrical Insulation and Dielectric Phenomena, IEEE, 2013, pp. 148–151.
[21] Q. Fan, L. Lian, T. Guanyu, et al., Effect of thermal oxidative ageing on the molecular structure and tribological properties of polytetrafluoroethylene, Tribol. Int. 188 (2023) 108850.
[22] Z. Lian, X.Y. Li, H. Yu, Y. Feng, S.T. Li, Research on XLPE ageing evaluation based on terahertz time-domain spectroscopy, Insul. Mater. 56 (10) (2023) 98–106 (in Chinese).
[23] Z. Liu, J. Hao, R. Liao, J. Li, Z. Gao, Z. Liang, Morphological, structural, and dielectric properties of thermally aged AC 500 kV XLPE submarine cable insulation material and its deterioration condition assessment, IEEE Access 7 (2019) 165065–165075, https://doi.org/10.1109/ACCESS.2019.2953127.
[24] M.P. Bracciale, L. Capasso, F. Sarasini, J. Tirillò, M.L. Santarelli, Effect of aging on the mechanical properties of highly transparent fluoropolymers for the conservation of archaeological sites, Polymers 14 (5) (2022) 912.
[25] J.L. Suthar, J.R. Laghari, Dielectric breakdown studies of teflon perfluoroalkoxy at high temperature, J. Mater. Sci. 27 (7) (1992) 1795–1800.
[26] Fanon Julienne, Emmanuel Richaud, Degradation of PVDF-HFP matrix, Macromol. Symp. 405 (1) (2022).
[27] Klaus Lunkwitz, Uwe Lappan, Ulrich Scheler, Modification of perfluorinated polymers by high-energy irradiation, J. Fluor. Chem. 125 (6) (2004) 863–873.
[28] Fluoropolymers Product Group (FPG), Safe Handling Guide for Fluoropolymer Resins, PlasticsEurope, 2025.
[29] L. Tian, Z. Lv, J. Gu, N. Li, Q. Zhang, High thermal conductivity graphite nanoplatelet/UHMWPE nanocomposites, RSC Adv. 5 (2015) 36334–36339.
[30] X. Zhang, X. Cai, X. Xie, C. Pu, X. Dong, Z. Jiang, T. Gao, Y. Ren, J. Hu, X. Zhang, Anisotropic thermally conductive perfluoroalkoxy composite with low dielectric constant fabricated by aligning boron nitride nanosheets via hot pressing, Polymers 11 (10) (2019) 1638.
[31] Bohang Li, et al., Beyond graphene: anticorrosion performance of fluorographene-filled perfluoroalkoxy alkane composite coatings for condensing heat exchanges, Prog. Org. Coating 165 (2022) 106748.
[32] Carlos Henrique Romoaldo, et al., Recycling tetrafluoroethylene–perfluoroalkyl vinylether copolymer (PFA) using extrusion process, Macromol. Mater. Eng. 308 (2) (2023) 2200458.
[33] Xiao Lin Huang, Juan Martinez-Vega, David Malec, Morphological evolution of polytetrafluoroethylene in extreme temperature conditions for aerospace applications, J. Appl. Polym. Sci. 131 (2014) 3.
[34] J. Mihály, S. Sterkel, H.M. Ortner, L. Kocsis, L. Hajba, É. Furdyga, J. Minka, FTIR and FT-Raman spectroscopic study on polymer based high pressure digestion vessels, Croat. Chem. Acta 79 (2006) 497–501.
[35] Patrícia Giunchetti Strabelli, et al., Effects of sintering variables on the microstructure of isostatically pressed PTFE parts, Polímeros 24 (2014) 612–619.
[36] Francisco Vilaplana, Sigbritt Karlsson, Macromol. Mater. Eng. 4/2008, Macromol. Mater. Eng. 293 (4) (2008), 249-249.
[37] Fuzhi Song, Qihua Wang, Tingmei Wang, The effects of crystallinity on the mechanical properties and the limiting PV (pressure× velocity) value of PTFE, Tribol. Int. 93 (2016) 1–10.
[38] Bruno Fayolle, et al., Degradation-induced embrittlement in semi-crystalline polymers having their amorphous phase in rubbery state, J. Mater. Sci. 43 (22) (2008) 6999–7012.
[39] S. Kumar, T. Rath, R.N. Mahaling, et al., Study on mechanical, morphological and electrical properties of carbon nanofiber/polyetherimide composites, Mater. Sci. Eng. B 141 (1–2) (2007) 61–70.
[40] A. Dorigato, Y. Dzenis, A. Pegoretti, Nanofiller aggregation as reinforcing mechanism in nanocomposites, Procedia Eng. 10 (2011) 894–899.
[41] S.G. Kuzak, A. Shanmugam, Dynamic mechanical analysis of fiber-reinforced phenolics, J. Appl. Polym. Sci. 73 (5) (1999) 649–658.
[42] L. Li, et al., Dielectric response of PTFE and ETFE wiring insulation to thermal exposure, IEEE Trans. Dielectr. Electr. Insul. 17 (4) (2010) 1234–1241.
[43] Ingo Alig, et al., Ac conductivity and dielectric permittivity of poly (ethylene glycol) during crystallization: percolation picture, Polymer 47 (5) (2006) 1722–1731.
[44] Boyuan Liang, et al., Influence of thermal aging on dielectric properties of high voltage cable insulation layer, Coatings 13 (3) (2023) 527.
[45] Z. Shen, B. Liu, G. Wang, S. Li, J. Wang, J. Huang, H. Zhang, K. Zhou, Accelerated electrical ageing characteristics of 10 kV XLPE cable, Insul. Mater. 54 (2021) 60–66.

[46] Y. Zhou, R. Han, X. Zhang, Y. Mao, X. Li, B. Zhai, Broadband dielectric characteristics of PEEK material used for packaging press pack IGBT devices, in: 2020 4th International Conference on HVDC (HVDC), IEEE, 2020, pp. 8–13.
[47] Danyu Li, Siyi Xu, Jianxi Li, Effect of thermal oxygen aging on the crystallization and insulation properties of polyether ether ketone, J. Appl. Polym. Sci. 140 (16) (2023) e53745.
[48] Mohamad M. Ahmad, Salah A. Makhlouf, Kamal Khalil, Dielectric behavior and ac conductivity study of NiO/ Al2O3 nanocomposites in humid atmosphere, J. Appl. Phys. 100 (9) (2006).
[49] Andrew K. Jonscher, The 'universal'dielectric response, nature 267 (5613) (1977) 673–679.
[50] Victor Henri, et al., Ageing of polyimide under thermal stress: relaxational effects and charge transport, Polym. Degrad. Stabil. 186 (2021) 109524.
[51] F.C. Cheng, Insulation thickness determination of polymeric power cables, IEEE Trans. Dielectr. Electr. Insul. 1 (4) (Aug. 1994) 624–629.
[52] P.K. Cheo, R. Luther, J.W. Porter, Detection of voids and contaminants in polyethylene insulated cable utilizing a fir laser beam, IEEE Trans. Power Apparatus Syst. 102 (3) (March 1983) 521–526.
[53] Fluoropolymers Product Group (FPG), Guide to the Safe Handling of Fluoropolymer Resins, 2019. Version 5.